

Chapter 6

Engineering the Magnetolectric Response in Piezocrystal-Based Magnetolectrics: Basic Theory, Choice of Materials, Model Calculations

João V. Vidal, Andrey A. Timopheev, Andrei L. Kholkin
and Nikolai A. Sobolev

Abstract This chapter presents a theoretical basis of the anisotropic magnetolectric (ME) effect in tri-layers of metglas and piezoelectric (PE) single crystals. The properties of various common PE and magnetostrictive substances are discussed, and arguments for the choice of the most appropriate materials are made. A linear description of the ME effects in terms of electric, magnetic and elastic material fields and material constants is presented. An averaging quasi-static method is used to illustrate the relation between the material constants, their anisotropy and the transversal direct ME voltage and charge coefficients. Subsequently, the aforementioned model is employed in the calculation of the maximum expected direct ME voltage coefficient for a series of tri-layered Metglas/Piezocrystal/Metglas composites as a function of the PE crystal orientation. The ME effects are shown to be strongly dependent on the crystal orientation, which supports the possibility of inducing large ME voltage coefficients in composites comprising lead-free PE single crystals such as LiNbO_3 , LiTaO_3 , $\alpha\text{-GaPO}_4$, $\alpha\text{-quartz}$, langatate and langasite through the optimization of the crystal orientation.

J.V. Vidal · A.A. Timopheev · N.A. Sobolev
Departamento de Física & I3N, Universidade de Aveiro, 3810-193 Aveiro, Portugal

A.L. Kholkin
Departamento de Física & CICECO, Universidade de Aveiro, 3810-193 Aveiro, Portugal

A.L. Kholkin
Institute of Natural Sciences, Ural Federal University, 620000 Ekaterinburg, Russia

N.A. Sobolev (✉)
National University of Science and Technology “MISiS”, 119049 Moscow, Russia
e-mail: sobolev@ua.pt

6.1 Introduction

6.1.1 The Magnetolectric Effect

The linear magnetolectric effect (ME), according to the original definition outlined by Debye in 1924–1926 [1], is described as the linear induction of a polarization, \mathbf{P} , in a material, in response to an applied magnetic field, \mathbf{H} . This is called the direct ME effect also designated by the acronym ME_H . In the same way, the converse ME effect (ME_E) is defined as the induction of a magnetization, \mathbf{M} , in a material as a result of an applied electric field, \mathbf{E} . These two relations can be expressed to the first order in the following way (in SI units) [2–5]:

$$P_i = \alpha_{ij}H_j; \quad (6.1)$$

$$\mu_0 M_i = \alpha_{ji}E_j, \quad (6.2)$$

where α indicates the linear ME susceptibility tensor (rank-2 tensor expressed in units of s/m), and μ_0 is the magnetic permeability of empty space. We note that the summation of the repeated index variables (i and j) over all of their integer values in tridimensional space is implicit in the above equations following the Einstein notation. Symbols in bold, on the other hand, represent vector or tensor fields.

The ME effect has given rise to a lot of interest in the scientific community over the past two decades, driven by the possibility of new and promising multifunctional device paradigms and also by the demand for a greater understanding of the fundamental physics associated with solid materials. This interest is evidenced by the large number of review articles related to developments in the field of the ME effect published in recent times [4–26].

Theoretical physical models are highly important because they allow us to draw valuable conclusions and predictions about the nature of the ME effect. Since early times, an important inequality for the ME single-phase materials has been drawn from a thermodynamic treatment. It states that [27, 28]:

$$\alpha_{ij} < \left({}^e\chi_{ii} {}^m\chi_{jj} \right)^{\frac{1}{2}} \quad (6.3)$$

where ${}^e\chi_{ii}$ and ${}^m\chi_{jj}$ are the electric and magnetic susceptibility tensor coefficients, respectively. The inequality (1.3) indicates the existence of a well-defined upper bound for all components of the α tensor. Although this limit is much higher than the experimentally measured values for all known ME materials [29], it still represents a severe limitation on the magnitude of the linear ME response in single-phase materials (i.e., multiferroics) [30, 31]. This is due to a chemical contraindication to the simultaneous occurrence of a high permittivity and permeability in the same material and results in part from a large intrinsic difficulty in electrically polarizing magnetic ions [32]. Furthermore, by arguments from the group theory, it can also be shown that the static linear ME effect may only be

observed in media that are neither symmetrical with respect to the space inversion operation (i.e., systems without a center of symmetry) nor with respect to the time reversal (i.e. systems with a magnetic ordering) [30–33]. Therefore, the ME effect is allowed only in 58 out of the 122 magnetic point groups [34]. A more general approach to the ME coupling may include higher-order contributions (describing the so-called secondary ferroics), parameterized by tensors such as β (ME effect induced by the \mathbf{H} field) or γ (ME effect induced by the \mathbf{E} field), both of rank-3, as can be seen by the general electromagnetic free energy expansion of a material [5, 35]:

$$F(\mathbf{E}, \mathbf{H}) = F_0 - \mathbf{P}_i^S \mathbf{E}_i - \mathbf{M}_i^S \mathbf{H}_i - \frac{1}{2} \varepsilon_0 \varepsilon_{ij} \mathbf{E}_i \mathbf{E}_j - \frac{1}{2} \mu_0 \mu_{ij} \mathbf{H}_i \mathbf{H}_j - \alpha_{ij} \mathbf{E}_i \mathbf{H}_j - \frac{1}{2} \beta_{ijk} \mathbf{E}_i \mathbf{H}_j \mathbf{H}_k - \frac{1}{2} \gamma_{ijk} \mathbf{H}_i \mathbf{E}_j \mathbf{E}_k - \dots \quad (6.4)$$

However, the linear term α_{ij} is generally the dominant contribution to the ME effect, and thus much of the current research in this area is directed towards the study of this linear effect.

Up to date, the ME effect has already been observed in several different types of materials [6, 7]. Two major classes of ME compounds can, however, be distinguished: single-phase ME materials (ME multiferroics) and ME composite materials which incorporate both piezoelectric (PE) and magnetostrictive (MS) materials in some manner. These composites may also integrate non-electric and non-magnetic compounds such as organic polymers and even multiferroic materials. Only the magnetoelectric composites will be explored in detail in this chapter, with the multiferroic compounds standing outside of its scope.

6.1.2 Magnetoelectric Composites

The bulk ME composite materials constitute a class of structures that incorporate both ferroelectric and ferri/ferromagnetic compounds [5, 6, 30]. The demand for these types of materials is essentially guided by the prospect of being able to control their internal charge distribution through the action of an applied magnetic field or, alternatively, their spin distribution by an electric field, thus allowing the development of new forms of multifunctional devices [8]. A ME coupling of large magnitude is therefore essential in order for them to be useful in efficient practical applications. Some of their most promising future applications may include [6, 7, 12, 23]: DC and AC magnetic field sensors, electric current sensors, multiple-state memories, RAM-like magnetic memories, micro-sensors in read-heads, transformers, spinners, diodes, optical devices that generate spin waves and electrically tunable microwave devices.

For the particular case of single-phase multiferroic compounds it has been known that the ME coupling constitutes a very rare phenomenon, usually being only observable at very low temperatures (low Curie and/or Néel temperatures for the electric and magnetic ordering) [6, 7, 19]. Furthermore, the single phase materials are commonly characterized by low values of the ME coupling coefficient ($\alpha_E \approx 0.4 - 20 \text{ mV}/(\text{cm}\cdot\text{Oe})$) [16, 17], in part due to the limits imposed by inequality (1.3). On the other hand, composite materials generally exhibit ME responses orders of magnitude stronger even at room temperature and, therefore, are currently much closer to commercial applications in new devices [6, 12]. Another major advantage of this configuration is associated with its enlarged manufacture flexibility. In fact, in order to manipulate the ME behavior of a composite, several parameters may be individually tuned including [6, 7, 12, 36]: (i) the properties of the constituent phases (e.g. PE and piezomagnetic coefficients, permittivity, permeability, elastic constants, electric resistivity, loss tangents, etc.); (ii) the volume and geometrical arrangement of the various phases (e.g. particulate or laminate structures, volume fraction between phases, layer thickness, grain size, rod diameter, etc.); (iii) the quality of the coupling between interfaces (e.g., structural compatibility between materials; synthesis techniques employed such as sintering, sol-gel method, hot-pressing, tape-casting, solid-state reaction or other physical/chemical deposition techniques; binding substances used such as epoxy, polymeric matrix, cyanoacrylate glue, etc.); (iv) the modes of operation (i.e. relative orientation between the applied/measured electric and magnetic fields, static or dynamic fields, charge, i.e. short-circuit, or voltage, i.e. open-circuit, measurements, frequency of the magnetic or electric modulation fields, etc.); (v) the processing techniques (e.g., pre-poling, pre-magnetizing, heat treatments, etc.); and (vi) the use of bulk phases or nanostructures such as thin films (which can give rise to new exotic effects).

To better understand the origin of the ME effect in PE/MS composite systems, we first take a look at the concept of physical properties resulting from the combination of distinct single-phase compounds. Here, it is known that composite systems may exhibit properties similar to those of their constituent phases but also give rise to completely new ones, absent in the parent compounds. The sum and scaling properties are part of the first class, while the product properties are associated with the former [7, 17, 37]. Thus, the ME effect in composite materials is in fact an extrinsic product property resulting from the interaction between PE and MS constituent phases [13, 17, 38]. The mechanism of the direct ME (ME_H) effect is as follows: the MS material is initially deformed as a result of the application of an external magnetic field (H). Part of this elongation/contraction (quadratic in the field) is then transferred to the PE phase leading to an elastic straining (S) and subsequently to the induction of a macroscopic electric polarization (P) due to the stress (T) driven PE effect. It is obvious that the reciprocal effect may also take place (converse ME effect or ME_E effect). In this case, an external electric field (E) induces a deformation of the PE component elongating or contracting it. This strain is then transmitted to the MS phase through a mechanical coupling between components. Thus, the magnetic phase experiences a magnetization (M) change

induced by the electric field. In summary, we just saw how a composite material can be characterized by a new property, the ME coupling, which is manifested by the appearance of a polarization (magnetization) in response to an externally applied magnetic (electric) field. Roughly speaking, the direct and converse ME effects may then be written under the form of the products [39]:

$$\begin{aligned} \text{ME}_H \text{ effect} &= \frac{\text{Electrical}}{\text{Mechanical}} \times \frac{\text{Mechanical}}{\text{Magnetic}}; \text{ME}_E \text{ effect} \\ &= \frac{\text{Magnetic}}{\text{Mechanical}} \times \frac{\text{Mechanical}}{\text{Electrical}}, \end{aligned}$$

where *Electrical/Mechanical* and *Mechanical/Magnetic* represent, respectively, the generation of PE charge ($d_{ij} = \partial D_i / \partial T_j$) and the MS deformation ($q_{ij} = \partial S_j / \partial H_i$), while *Magnetic/Mechanical* and *Mechanical/Electrical* represent the piezomagnetic induction ($q_{ij} = \partial B_i / \partial T_j$) and the PE deformation ($d_{ij} = \partial S_j / \partial E_i$). With this concept of product properties in mind, the effective short-circuit ($E_i = 0$) ME coefficient can then be approximately expressed as [6, 40]:

$$\alpha_{Qij} = \partial D_i / \partial H_j = (\partial D_i / \partial T_k)(\partial T_k / \partial S_l)(\partial S_l / \partial H_j) = k_c d_{ik} s_{kl}^{-1} q_{jl} \quad (6.5)$$

where k_c is a coupling factor ($0 \leq |k_c| \leq 1$) that quantifies the efficiency of the transference of strain between phases (i.e. the ratio between the strain transferred to the PE/MS phase and the strain generated in the MS/PE phase by the external field) and depends on the fraction and connectivity between phases [41]. This expression indicates that the ME coupling should be favored by large PE coefficients (d_{ij}), piezomagnetic coefficients (q_{ij}), the inverse of averaged effective elastic compliances (s_{ij}^{-1}) and coupling factors (k_c). Consequently, the ME effect in composite materials is a coupling between electrical and magnetic fields mediated by an elastic interaction, and is therefore an extrinsic property generated from separate compounds which do not exhibit any ME behavior by themselves.

Since the ME interaction between different phases is a complex process, the ME response observed in composite materials will not simply be linear as in the case of most multiferroic compounds [7, 12]. In composites, the ME effect is actually a dynamic effect, and a large linear response can only be observed with an AC field (electric or magnetic) oscillating in the presence of a given DC field. In addition to the nonlinear response due to the quadratic effect of magnetostriction, generally the ME coupling in composites also displays a hysteretic nature [17]. Therefore, under open-circuit conditions, a dynamic direct ME voltage coefficient $\alpha_{Eij} = \partial E_i / \partial H_j$ is used as a figure of merit. For a traction-free composite the relation $\alpha_{ik} = -\varepsilon_0 \varepsilon_{rij} \alpha_{Ejk}$ can be proven [40, 42, 43], where α_{ij} represents its effective dynamic ME susceptibility, ε_{rij} the effective relative dielectric permittivity and ε_0 the permittivity of empty space. α_{Eij} is typically specified in technical units of V/(cm·Oe) which can be converted to SI units (V/m)/(A/m) through a multiplication by a factor of $4\pi/10$.

This coefficient is usually defined for a magnetic AC modulated field ($\delta H_i(t) = \delta H_i \cdot \sin(\omega t)$) with small amplitude (δH up to approximately 1 Oe) and with a frequency ($f = \omega/2\pi$) of up to about 1 MHz, superimposed on a larger (up to, say, 20 kOe) magnetic DC bias field (\mathbf{H}) [7]. The amplitude of the ME induced AC voltage (δV_i) measured between two electrodes in the sample should then be proportional to the amplitude of the AC magnetic field in any detection circuit, thus establishing an analogy with the linear ME response observed in single-phase compounds. Finally, in order to quantify the dynamic ME coefficients, one measures the ME voltage induced in a sample by the magnetic field and then uses the relation $\alpha_{Eij} = \delta V_i / (t \cdot \delta H_j)$, which is valid for small enough δH_j [44] and where t is the effective distance between electrodes generally equal to the thickness of the PE. In practice, two particular cases of this coefficient are commonly studied in the literature [6, 7, 12, 28]: (i) the longitudinal T-T ME voltage coefficient (α_{E33}), and (ii) the transversal L-T ME voltage coefficient (α_{E31} or α_{E32}). Additionally to α_E , another ME coefficient can be used to describe the direct ME effect in composites under distinct operation conditions. This is the so called charge ME coefficient (α_Q), usually measured under short-circuit conditions, and it quantifies the amount of charge generated as a function of the applied magnetic field i.e. $\alpha_{Qij} = \partial D_i / \partial H_j \propto -C \alpha_{Eij}$, where C is the low-frequency capacitance of the composite [45–47]. This coefficient can be measured directly by an electrometer or ammeter or indirectly as a voltage from the output of a charge amplifier and is particularly important for applications in low-noise (<5 pT/Hz^{1/2}) and low-frequency (<1 Hz) magnetic field sensors [46, 48, 49]. Alternatively, a less common converse ME coefficient, $\alpha_{Bij} = \partial B_i / \partial E_j$, can also be quantified by measuring the magnetic response of a sample when an electric field is applied to it (e.g., through a change in the amplitude of the magnetization induced by an applied voltage, a variation in hysteretic magnetization curves, a change in the magnetic anisotropy or a shift of ferromagnetic resonance absorption peaks) [20]. The analysis of this parameter can be important, e.g., for applications in inductances and electrically controlled microwave devices [23].

Composite materials can be manufactured with a variety of geometries and compositions. Here, a certain phase may take the shape of particles, fibers/rods, layers or three-dimensional arrays which, in the Newnham notation, can be denoted by the indices 0, 1, 2 and 3, respectively [50]. In this way, the notation 2-2, for example, indicates a two-phase composite consisting of alternating layers of different materials. As for its composition, bi-phasic composites contain a ferroelectric phase, usually BiFeO₃ (BFO), BaTiO₃ (BTO), PbTiO₃ (PTO), Pb(Zr,Ti)O₃ (PZT), (1-x)[PbMg_{1/3}Nb_{2/3}O₃]-x[PbTiO₃] (PMN-PT) or (1-x)[PbZn_{1/3}Nb_{2/3}O₃]-x[PbTiO₃] (PZN-PT), and a ferromagnetic phase, generally consisting of ferrites or magnetic alloys such as NiFe₂O₄ (NFO), CoFe₂O₄ (CFO), Fe₃O₄, La_{1-x}Sr_xMnO₃ (LSMO), Y₃Fe₅O₁₂ (YIG), Tb_xDy_{1-x}Fe₂ (Terfenol-D), Metglas (Fe-Ni-Co-B-Si-Mo), Permendur (Fe-Co-V) or Galfenol (Fe-Ga) [6, 14]. Table 6.1 summarizes some of the most important properties from the point of view of the ME coupling, of some of the most thoroughly investigated PE materials. PE ceramics, PZT in

Table 6.1 Main physical properties, relevant to the ME effect, of some common Z-cut piezoelectrics

	BaTiO ₃	LiNbO ₃	GaPO ₄	PZT-5	PZT-4	PZN-PT	PMN-PT	PVDF	NKN
d_{31} (pC/N)	-33	-0.85	-1.58 (d_{14})	-175	-109	-1280	≈700	16.5	-
d_{33} (pC/N)	94	6	4.37 (d_{11})	400	300	2000– 2500	2000	-33	158
ϵ_{r33}^T	132	85.2	5.38 (ϵ_{r11}^T)	1750	1350	7200	5000	10	-
T_c (°C)	152	1210	900	360	320	163	80	129	415
ρ (g/cm ³)	6	4.63	3.57	7.7	7.6	8.2	7.8	1.78	-
Q_m	-	-	-	80	500	-	-	4	234
k_{33}^l	0.63	0.17	0.15 (k_{11}^l)	0.72	0.68	0.94	≈0.9– 0.94	0.19	0.46
References	[55, 56]	[57]	[58, 59]	[14]	[14]	[14, 60, 61]	[14, 62]	[14]	[24]

Here, d_{31} and d_{33} represent the PE strain coefficients, ϵ_{r33}^T is the dielectric relative permittivity, T_c the Curie temperature, ρ the mass density, Q_m the mechanical quality factor (i.e. 2π times the energy stored divided by the energy dissipated per cycle for a given fundamental resonance mode expressed as $\sqrt{L_1/C_1}/R_1$, where L_1 , C_1 and R_1 are respectively the series inductance, capacitance and resistance of the equivalent electrical circuit of the PE vibrator [54]) and k_{33}^l the electromechanical coupling factor for a longitudinal oscillation (i.e. the square-root of the ratio between delivered mechanical or electrical energy and total absorbed energy in this case given by $d_{33}/\sqrt{s_{33}^E e_{33}^T}$ [54])

particular, have been extensively studied and shown to provide a strong ME coupling thanks to their relatively large PE and electromechanical coupling coefficients [51–53]. Other compounds commonly used as the PE phase in ME composite materials are PMN-PT and PZN-PT [14, 22, 53]. These materials have PE and electromechanical characteristics superior to those of PZT but, on the other hand, are associated with low Curie temperatures and low fracture toughness, which severely limits their practical applications [14]. The polymer PVDF is another common material, less attractive from the point of view of the PE accumulation of charge (though it has a relatively large PE strain coefficient), but which has the advantages of being elastically soft and having a high electrical resistivity and resistance to solvents [14]. Some early research also has pointed out to the possibility of using single-crystalline PE materials exhibiting considerably better performances [22]. Nevertheless, the PE ceramics based on PZT, PMN-PT and PZN-PT still possess the best known dielectric and PE properties and thus are in the prime position for future applications in actuators, sensors and resonators [14, 22, 51–53]. However, lead (Pb) featured in these compounds represents a serious environmental problem, and therefore a great deal of current research is focused on identifying lead-free PE compounds which could serve as alternatives to the former [24]. In recent times, many developments have been made in this direction with the appearance of a series of new “clean” piezoelectrics. Among these, ceramics based on the compound (Na,K)NbO₃ (NKN) (e.g., solid solutions of NKN-LiNbO₃,

Table 6.2 Main physical properties, relevant to the ME effect, of some important MS materials

	NiFe ₂ O ₄	Terfenol-D	Permendur	Galfenol	Metglas 2605
λ_s (ppm)	27	1400	70	200	40
q_{33} (ppm/Oe)	≈0.18	≈1–2	≈1	≈1.5	≈4.0
μ_{r33}^T	20	≈6–10	2300	20	>40 000
T_C (°C)	535	380	940	670	395
ρ (g/cm ³)	5.37	7.8	8.2	7.7	7.18
σ (S/m)	1.00×10^{-6}	1.72×10^6	2.38×10^6	1.67×10^6	7.69×10^5
References	[14, 74]	[14, 52, 72, 75]	[76–78]	[14, 79, 80]	[14, 68, 72]

Here, λ_s is the saturation magnetostriction, q_{33} the piezomagnetic coefficient, μ_{r33}^T the relative magnetic permeability, ρ the mass density, σ the electrical conductivity and T_C the Curie temperature

NKN-LiTaO₃, NKN-LiSbO₃, NKN-Li(Nb,Ta,Sb)O₃, NKN-BaTiO₃, NKN-SrTiO₃ or NKN-CaTiO₃) have received considerable attention for two main reasons [24]: (i) their PE properties stay unchanged over a wide temperature range and (ii) there are numerous possibilities of chemical substitution in the compounds.

Similarly, the main properties of the most attractive MS materials are summarized in Table 6.2. Here, one can identify the greatest advantage of ferrites with respect to metallic alloys when employed in particulate ME composites, viz., its high electrical resistivity. This is critical when one seeks to obtain MS phases capable of withstanding an electric displacement field on 0–3 particulate or 1–3 fiber/rod composites because, otherwise, there would be a large leakage of current through the compound thus nullifying the charge built-up. NiFe₂O₄, in particular, is the ferrite with the largest saturation magnetostriction (λ_s) currently known, while also possessing good mechanical properties. Despite its small magnetostriction in relation to alloys, NiFe₂O₄ is still widely used in ME composites and could find applications, e.g., in microwave devices [14]. However, in 2-2 laminate composites, layers of the MS phase tend to be interspersed by layers of the PE phase, commonly associated with a large electrical resistivity. In this case the leakage of current through the thickness of the composite is minimized, so that the MS phases are no longer required to have high resistivities. Therefore, the research on ME composites in the last decade has been strongly focused on composite laminates containing the MS alloy Terfenol-D (Tb_{0.3}Dy_{0.7}Fe_{1.92}/Pb(Zr_{0.52}Ti_{0.48})O₃) [12, 63–67]. Among all known magnetic materials, Terfenol-D is still the one with the highest saturation magnetostriction [6]. On the other hand, this compound is very expensive and brittle, as well as exhibiting high losses at high frequencies (≥100 kHz) caused by eddy currents. As in all alloys, it also has a low electrical resistivity and cannot be co-sintered with ferroelectric oxides [14]. Also, its low magnetic permeability ($\mu_r \approx 3–10$) and large saturation field require high magnetic fields (typically above 1 kOe) in order to maximize the ME coupling coefficients, making it unsuitable for low-field applications [6, 23]. Consequently, the study of other lower-cost magnetic alloys such as Permendur (Fe–Co–V), Galfenol (Fe–Ga) or Metglas (Fe–Ni–Co–B) is of great interest [51, 68–70]. Currently, one of the most promising MS alloys is

Metglas, mainly because of its huge relative magnetic permeability ($\mu_r > 10\,000$), large piezomagnetic coefficient ($q_{33} \approx 4.0$ ppm/Oe) and reasonable saturation magnetostriction ($\lambda_s = 40$ ppm) [14]. Different types of this compound consist of soft Fe-, Co- or Fe–Ni-based amorphous alloys, also containing small quantities of B and in some cases Si and Mo, fabricated by a rapid solidification process [71]. This process provides it with unique magnetic properties such as a very high permeability and a very low coercivity and magnetic anisotropy. Despite its smaller saturation magnetostriction when compared to Terfenol-D, ME composites of Metglas can still display very large ME couplings. This is because, as will be shown later, the ME dynamic coefficients are proportional to the linear piezomagnetic constants ($q_{ij} = \partial S_j / \partial H_i = \partial \lambda_j / \partial H_i$) and not to the saturation magnetostriction (λ_s). In fact, Metglas constitutes the material with the largest known piezomagnetic coefficient, $q_{33} \approx 4$ ppm/Oe (in the case of the 2605SA1 alloy) [68, 72], being approximately twice the one observed for Terfenol-D [52]. It also has a high transversal coefficient of $q_{11} + q_{12} \approx 1.5$ ppm/Oe [73]. Additionally, its very high permeability ensures a high concentration of magnetic flux and, therefore, a saturation of the magnetization and magnetostriction at very low magnetic fields of ca. 10 Oe. Consequently, its piezomagnetic and ME coefficients, when incorporated into a ME composite, generally attain maximum values at low magnetic fields.

Since the initial research and until this day, the ME laminate composites have attracted a particularly large interest because of their large ME coefficients, due to large PE and MS coefficients and an absence of current leakage, which have paved the way to several promising applications. Thus, a wide variety of laminar geometries [66, 67, 81–83], synthesis/binding techniques [82–84] and operation modes [63–66, 85, 86] have already been studied in detail. With regard to their geometry, the most frequently employed laminate composites are based on simple structures of only two or three rectangular or disk shaped layers (i.e. sandwich structures) [6]. These structures are the most investigated primarily for their ease of manufacture and for exhibiting, in general, very intense ME effects with coefficients usually in the range from 0.05 to 45 V/(cm·Oe) in the quasi-static regime (i.e. under off-resonance conditions) [16, 18, 22, 23, 26].

When an oscillating AC magnetic field is applied to a ME composite, its ME response oscillates with the fundamental frequency and higher harmonics of this field. In particular, a large increase in the magnitude of the ME effect is expected whenever the frequency matches one of the natural electrical, magnetic or mechanical modes of resonance of the structure [20, 87–89]. Both phases of the composite can exhibit these phenomena. These are known as electromechanical resonance (EMR), for the case of the PE phase, and ferromagnetic resonance (FMR), for the case of the magnetic phase.

The EMR occurs when a characteristic mechanical eigenmode of the PE phase is indirectly excited by the varying magnetic field [88]. This field produces a periodic strain in the MS phase which is then transferred to the PE phase. A conventional mechanical resonance of the PE can then be observed when the elastic vibration frequency coincides with a natural frequency (or one of its harmonics) of the

system. This frequency depends on the effective material parameters and geometry of the PE. Thus, a large oscillation amplitude of the standing wave in this layer will also give rise to a large polarization/voltage through the PE effect. Theoretical models based on equivalent circuits for the composites have shown that the ME coefficient at resonance is approximately Q_m times larger than that observed off resonance, where Q_m is the effective mechanical quality factor of the composite [22]. It is also possible to show that the extensional length-resonance frequencies of a traction-free laminate composite with the shape of a long bar (i.e., with a length much larger than its width and thickness) can be given by $f_{ln} = (2n - 1)/2\ell\sqrt{\rho s_{11}}$ [90], where $n \in \mathbb{N}$ is the harmonic number, ℓ the length of the PE bar, ρ its mass density and s_{11} the longitudinal elastic compliance along the length direction (here assumed to be X as in Fig. 6.1a) [14]. For laminate composites with lengths of about 1 cm and thicknesses of about 1 mm, fundamental in-plane extensional EMRs are generally observed in the range from 200–400 kHz, while fundamental thickness extensional EMRs are commonly found in the range from 2–4 MHz [91–93]. For the case of a PE with a more complex geometry, however, additional types of EM modes are expected to be found including shear and flexural modes, mainly in the case of symmetrical laminate composites, and bending modes, mainly in the case of asymmetrical laminate composites. As in the extensional case, for a traction-free long-bar shaped PE the n first bending resonant modes should be observed at $f_{bn} = \beta_n^2 t / 2\pi\ell^2 \sqrt{12\rho s_{11}}$ (with $\beta_1 \approx 4.730$, $\beta_2 \approx 7.853$, $\beta_3 \approx 10.996$, $\beta_4 \approx 14.137$, etc.) [90], where t is the thickness of the PE. The fundamental bending modes are typically observed in the range from 40–80 kHz in PE plates with lengths of approximately 1 cm and thicknesses of about 1 mm. Under bending EMR conditions, ME voltage coefficients as large as 737 V/(cm·Oe) have thus been detected at low frequencies in ME thin film layered composites [94] and up to 16 kV/(cm·Oe) in specially designed ME ferromagnetic-elastic-PE cantilever structured composites [95–97].

The FMR phenomenon involves the resonant absorption of a microwave by the ferromagnetic component of the composite when subjected to some magnetic bias field. An electric field (E_j) applied to the composite thus straining the ferromagnetic

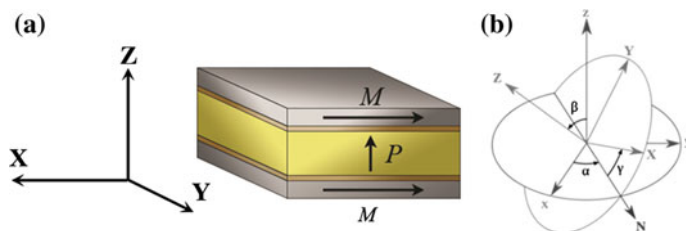


Fig. 6.1 **a** Representation of a tri-layered ME composite operating in the transversal L-T mode (i.e. longitudinal or in-plane magnetization, M , of the MS layers and transversal or out-of-plane polarization, P , of the PE layer). **b** Euler angles scheme used in the rotation of the crystallographic frame of a single crystal to the laminate frame of figure **a** [111]

phase may consequently shift this resonant magnetic field [88, 98]. A very large ME coupling has additionally been predicted for a superposition of EMR and FMR, in which case it is called magnetoacoustic resonance (MAR) [88]. In general, one expects to observe EMR for frequencies of the order of 100 kHz, FMR of the order of 10 GHz and antiferromagnetic resonances of the order of 100 GHz [6, 7, 12, 26]. The latter two make the ME laminates very promising from the point of view of microwave devices.

6.2 Theory of the Magnetoelectric Effect

6.2.1 Piezoelectricity and Magnetostriction

The phenomena of piezoelectricity and magnetostriction can be mathematically described by a model derived from thermodynamics, electrodynamics and continuum mechanics. The set of equations obtained including Maxwell's equations, conservation of linear momentum, angular momentum, energy and mass (in the non-relativistic approximation) thus depend on the choice of the thermodynamic potential. Starting with a PE system and considering isothermal and adiabatic conditions and ignoring higher-order effects, the system's Gibbs free energy may be described by [54, 99–101]:

$$G(\mathbf{E}, \mathbf{T}) = -\frac{1}{2} {}^p s_{ijkl}^E {}^p T_{ij} {}^p T_{kl} - d_{kij} {}^p E_k {}^p T_{ij} - \frac{1}{2} (\varepsilon_{kl}^T - \varepsilon_0 \delta_{kl}) {}^p E_k {}^p E_l, \quad (6.6)$$

where the Einstein summation convention is used. Here, ${}^p s_{ijkl}^E$ is an element of the elastic compliance tensor (a rank-4 tensor), d_{kij} the PE strain coefficient (a rank-3 tensor), ε_{kl}^T the dielectric permittivity (a rank-2 tensor), ${}^p T_{ij}$ the elastic stress (a rank-2 tensor), and ${}^p E_k$ the electric field (a vector). The superscripts E and T in the material constants indicate that those are defined under the conditions of a constant electric field or stress, respectively. Throughout the rest of this chapter, the subscripts i, j, k and l will range over the integers 1, 2 and 3, whereas the subscripts a, b, c and d over just 1 and 2. The superscript p on the constants and variables is meant to remind us that we are dealing with a PE medium. Through the partial differentiation of the G potential, the linear constitutive equations of piezoelectricity are obtained as [54, 99–101]:

$${}^p D_k = \varepsilon_0 {}^p E_k - \frac{\partial G}{\partial {}^p E_k} = \varepsilon_{kl}^T {}^p E_l + d_{kij} {}^p T_{ij}; \quad (6.7)$$

$${}^p S_{ij} = -\frac{\partial G}{\partial {}^p T_{ij}} = {}^p s_{ijkl}^E {}^p T_{kl} + d_{kij} {}^p E_k, \quad (6.8)$$

where pD_k is the electric displacement (a vector) and ${}^pS_{ij}$ is the elastic strain (a rank-2 tensor).

All of the tensor parameters for a given property of the material mentioned so far are mathematical objects that change with the coordinate system in a predictable way and obey certain symmetry relations, which considerably reduces the number of their independent components. Those symmetry relations have three basic sources [102]: the symmetry of the partial differential equation (PDE) that defines the property, the symmetry of the tensor variables which determine the property, and the symmetry of the material that exhibits the property (i.e., its point group). The first kind of symmetry limits the number of independent elements of the tensor properties which are defined by repeated differentiation. An example of this is the PE coefficient, where $d_{kij} = d_{kij}^E = (\partial D_k / \partial T_{ij})_E = -\partial^2 G / \partial T_{ij} \partial E_k = -\partial^2 G / \partial E_k \partial T_{ij} = (\partial S_{ij} / \partial E_k)_T = d_{kij}^T$, the dielectric permittivity $\varepsilon_{kl}^T = (\partial D_k / \partial E_l)_T = \varepsilon_0 \delta_{lk} - \partial^2 G / \partial E_l \partial E_k = \varepsilon_0 \delta_{lk} - \partial^2 G / \partial E_k \partial E_l = (\partial D_l / \partial E_k)_T = \varepsilon_{lk}^T$, and the compliance $s_{ijkl}^E = (\partial S_{ij} / \partial T_{kl})_E = -\partial^2 G / \partial T_{ij} \partial T_{kl} = -\partial^2 G / \partial T_{kl} \partial T_{ij} = s_{klij}^E$. The theory of linear elasticity yields $S_{ij} = (1/2)(\partial u_i / \partial x_j + \partial u_j / \partial x_i)$, where u_i are the displacement vectors along the x_i Cartesian directions, so that $S_{ij} = S_{ji}$, thus reducing the number of independent variables to 6. Furthermore, the conservation of angular momentum also implies that $T_{ij} = T_{ji}$. Consequently, taking into account this symmetry of the tensor variables that determine the properties $d_{kij} = (\partial D_k / \partial T_{ij})_E$ and $s_{ijkl}^E = (\partial S_{ij} / \partial T_{kl})_E$, one further identifies the following symmetry relations: $d_{kij} = d_{kji}$ and $s_{ijkl}^E = s_{jikl}^E = s_{ijlk}^E = s_{jilk}^E$. In summary, it follows from these two sources of intrinsic symmetry that the dielectric permittivity has a maximum of 6 independent constants, whereas the dielectric coefficient and compliance have a maximum of 18 and 21, respectively. To simplify the manipulation of these expressions, a special notation known as Voigt's notation is commonly used in literature. Here, the ε^T , \mathbf{d} and \mathbf{s}^E tensors are represented as 3×3 , 3×6 and 6×6 matrices, where the ij subscripts are reduced to a single subscript (m or n) using the substitutions $ij = 11 \rightarrow 1$, $ij = 22 \rightarrow 2$, $ij = 33 \rightarrow 3$, $ij = 23, 32 \rightarrow 4$, $ij = 13, 31 \rightarrow 5$, $ij = 12, 21 \rightarrow 6$. Other rules of conversion into this matrix notation, which must be taken into account, are [54, 103]: $S_m = S_{ij}$, when $m = 1, 2$ or 3 ; $S_m = 2S_{ij}$, when $m = 4, 5$ or 6 ; $s_{mn}^E = s_{ijkl}^E$, when both m and n are $= 1, 2$ or 3 ; $s_{mn}^E = 2s_{ijkl}^E$, when m or n are $= 4, 5$ or 6 ; $s_{mn}^E = 4s_{ijkl}^E$, when both m and n are $= 4, 5$ or 6 ; $d_{km} = d_{kij}$, when $m = 1, 2$ or 3 ; and $d_{km} = 2d_{kij}$, when $m = 4, 5$ or 6 . The values of these coefficients are frequently presented in literature in this notation. Taking all these symmetry considerations into account, the constitutive equations (6.7) and (6.8) can be written in the general matrix form [54, 99]:

$$\begin{bmatrix} S_m \\ D_i \end{bmatrix} = \begin{bmatrix} {}^pS_{mn}^E & d_{mj}^T \\ d_{in} & \varepsilon_{ij}^T \end{bmatrix} \begin{bmatrix} T_n \\ E_j \end{bmatrix} \quad (6.9)$$

where the superscript t indicates the transpose of the d Voigt matrix. Finally, it has to be noted that the symmetry of the material is also an important source of additional constraints on its tensor properties. From the symmetry of a system we know that there are a set of symmetry operations which will not change the material in any observable way, so that the material properties will be invariant under such operations. These operations are the ones that define the point group of the system. Thus, one sees that the material properties are in part governed by the point group symmetry of the material. More precisely, the Neumann principle states that [104] *The symmetry elements of any physical property of a crystal must include all the symmetry elements of the point group of the crystal.* In other words, the components of a tensor representing a property must remain invariant under any transformation of coordinates governed by a symmetry operation valid for the point group of the crystal. This also implies that a given physical property may only possess a higher or equal symmetry than that of the crystal. Therefore, a physical property must have a symmetry at least as high as one of the 32 conventional point groups or one of the 122 magnetic point groups to which the crystal belongs. Taking, e.g., the PE LiNbO_3 crystal corresponding to the point group $3m$, it is possible to show that it will be associated with at most 2 independent dielectric constants (ϵ_{11}^T and ϵ_{33}^T), 4 PE constants (d_{31} , d_{33} , d_{22} and d_{15}) and 6 compliance constants (s_{11}^E , s_{12}^E , s_{13}^E , s_{14}^E , s_{33}^E and s_{44}^E) [57]. A listing of all the 32 point groups and associated tensor properties can be found, e.g., in [104–106].

Most of the discussion mentioned above for PE materials can also be applied to piezomagnetic materials. The difference resides in the fact that, because magnetic fields are pseudovectors generated by currents and change sign under time inversion, magnetic properties will necessarily have more complex symmetries [102]. In fact, there is a whole set of additional point group symmetries for the magnetic properties as a consequence of current reversal. Therefore, while the simplest magnetic properties, such as the magnetic permeability and susceptibility, have the forms that are required by the basic crystallographic point group of the material, more complex properties, such as the ferromagnetic moment and the MS coefficients, do not. Those will instead have the form required by one of the 122 magnetic point groups. Assuming the same conditions as in the case of the PE material, the elastic Gibbs function for the MS material can also be derived. From it, the linear piezomagnetic constitutive relations follow [43, 107]:

$${}^m B_k = \mu_0 {}^m H_k - \frac{\partial G}{\partial {}^m H_k} = {}^m B_{0k}(\mathbf{H}_0) + \mu_{kl}^T(\mathbf{H}_0) {}^m H_l + q_{kij}(\mathbf{H}_0) {}^m T_{ij} \quad (6.10)$$

$${}^m S_{ij} = - \frac{\partial G}{\partial {}^m T_{ij}} = {}^m S_{0ij}(\mathbf{H}_0) + {}^m s_{ijkl}^E {}^m T_{kl} + q_{kij}(\mathbf{H}_0) {}^m H_k, \quad (6.11)$$

where ${}^m B_k$ is the magnetic induction (a vector) and ${}^m H_k$ the magnetic field strength (a vector). Also, ${}^m B_{0k}(\mathbf{H}_0) = {}^m B_k(\mathbf{H}_0) - \mu_{kl}^T(\mathbf{H}_0) {}^m H_{0l}$ and ${}^m S_{0ij}(\mathbf{H}_0) = \lambda_{ij}(\mathbf{H}_0) - q_{kij}(\mathbf{H}_0) {}^m H_{0k}$ where $\mu_{kl}^T(\mathbf{H}_0)$ is the magnetic permittivity (a rank-2 tensor), $q_{kij}(\mathbf{H}_0)$

the piezomagnetic coefficient (a rank-3 tensor), ${}^m B_k(\mathbf{H}_0)$ the magnetic induction and $\lambda_{ij}(\mathbf{H}_0)$ the magnetostriction all measured at a bias \mathbf{H}_0 magnetic field. The superscript m indicates the MS nature of the material to which (6.10) and (6.11) apply. It should be noted that, when obtaining these equations, the pseudo-piezomagnetic approximation was taken. This is because magnetostriction is approximately a quadratic effect (${}^m S_{ij} = b_{ijkl} M_k M_l$, where \mathbf{b} is the 6×6 magnetoelastic tensor), whereas piezomagnetism is a linear effect (${}^m S_{ij} = q_{kij} H_k$). However, for small variations of the applied \mathbf{H} field close to a bias field \mathbf{H}_0 , the slope $\partial S_{ij}^m / \partial H_k(\mathbf{H})$ of the magnetostriction curve is approximately constant in a small interval around \mathbf{H}_0 . Therefore the Taylor expansion of the magnetostriction curve around \mathbf{H}_0 may be truncated to first order as follows: ${}^m S_{ij}(\mathbf{T} = 0, \mathbf{H}) = \lambda_{ij}(\mathbf{H}) = \lambda_{ij}(\mathbf{H}_0) + \partial \lambda_{ij} / \partial H_k(\mathbf{H}_0) \cdot (H_k - H_{k0}) + (1/2) \partial^2 \lambda_{ij} / \partial H_k \partial H_l(\mathbf{H}_0) \cdot (H_k - H_{k0})(H_l - H_{l0}) + \dots \approx \lambda_{ij}(\mathbf{H}_0) + \partial \lambda_{ij} / \partial H_k(\mathbf{H}_0) \cdot (H_k - H_{k0})$, and thus the magnetostriction can be approximated in this region as a piezomagnetic effect with $q_{kij}(\mathbf{H}_0) = \partial \lambda_{ij} / \partial H_k(\mathbf{H}_0)$ [28, 108]. In practical applications, the magnetostriction is often used in this linear piezomagnetic regime with small applied AC magnetic fields. Similarly, a pseudo-paramagnetic approximation, where $\mu_{kl}^T(\mathbf{H}_0) = \partial B_k / \partial H_l(\mathbf{H}_0)$, is also assumed for the ferromagnetic material. Having taken this into consideration, one can therefore assume the validity of (6.10) and (6.11). Before advancing any further, one has to note that the assumption that the material coefficients in the constitutive equations are constants dependent only on the spatial coordinates and magnetic fields produces a very idealized model. In a more accurate description these coefficients should be complex functions of space, material fields, frequency, time and temperature thus taking into account the non-linearities, dispersion, losses, current state (e.g. remanent polarization/magnetization of the PE/MS phase, aging effects, etc.) and temperature dependence of the material's properties. A listing of all the linear dielectric, PE and elastic constants of the different piezoelectrics, measured under standard ambient conditions, can generally be easily found in literature.

6.2.2 Presentation of the Averaging Quasi-Static Method

In this Section we are going to estimate the maximum expected magnitude of the ME voltage coefficient for a series of tri-layered geometries of the type Metglas/PE/Metglas, where different single crystals are employed as the PE phase. To do this, a standard averaging low-frequency model (i.e., in the quasi-static regime), based on the constitutive equations, will be used. Being quasi-static it will naturally neglect high frequency effects such as electromechanical resonances, material dispersion and losses as well as eddy currents generated in the conductive phases.

The simultaneous resolution of the constitutive equations (6.7)–(6.8) and (6.10)–(6.11), taking into account the boundary conditions for the material interfaces,

allows one to obtain the ME voltage coefficient of the composite depending on its composition, microstructure, operating mode, etc. Currently, a number of analytical and numerical techniques are known which may be employed in solving these equations. In general, they allow estimations in terms of mean fields and are based on the formalism of Green's function [39] (multiple-scattering approach in the many-body theory) or on micromechanical methods [109]. More sophisticated models may include the quadratic effect of magnetostriction [110] and pyroelectric or pyromagnetic phenomena [109] in the constitutive equations.

In the quasi-static model, a square shaped tri-layered structure like the one shown in Fig. 6.1a is considered. Its constitutive elastostatic and electrostatic equations are solved assuming that all of the material fields are averaged constants in each layer up to the leading order. This limits the model to the study of purely extensional deformations thus excluding any kind of bending deformations which, however, are only significant for the case of asymmetrical composites such as bilayers. As we see, this composite is designed to operate in its L-T mode, i.e., with a magnetic field ($\delta H_j(t)$) applied along its longitudinal length direction (L) and with the voltage ($\delta V_3(t)$) measured across its transversal thickness direction (T). This L-T mode is generally associated with larger ME coefficients than the transversally magnetized and transversally poled (T-T) mode mainly because of the absence of the demagnetization effect (for thin enough layers) and also because the piezomagnetic coefficients tend to be larger for parallel magnetic and strain fields (q_{ii}), so that the in-plane strain component, which is transmitted to the PE phase, will be larger.

To set the boundary conditions, we start by assuming that there is no external traction applied to the system. Thus, the average tractions on the top and bottom surfaces of both phases (${}^m T_{3i}$), as well as the average tractions on the lateral surfaces (${}^p T_{ab}{}^p \nu + {}^m T_{ab}{}^m \nu$), are null. These two relations are expressed as [43, 107]:

$${}^m T_{3i} = {}^p T_{3i} = 0; \quad (6.12)$$

$${}^p T_{ab}{}^p \nu + {}^m T_{ab}{}^m \nu = 0, \quad (6.13)$$

where ${}^p \nu$ and ${}^m \nu$ are the volume fractions of the PE and MS phases, respectively. Taking into account that all layers have a square shaped surface with the same area (A), these fractions are given by ${}^p \nu = {}^p t / ({}^p t + 2{}^m t)$ and ${}^m \nu = 2{}^m t / ({}^p t + 2{}^m t)$, where ${}^p t$ is the thickness of the PE crystal and ${}^m t$ is the thickness of each one of the two magnetic layers. The continuity conditions at the interfaces between layers guarantee that ${}^m T_{3i} = {}^p T_{3i}$. Furthermore, a parameter known as the coupling coefficient, $k_c = ({}^p S_{ab} - {}^p S_{0ab}) / ({}^m S_{ab} - {}^p S_{0ab})$, is introduced [42]. This parameter describes the coupling quality at the interface between the PE and MS materials. In the expression of k_c , ${}^p S_{0ab}$ indicates the component of the strain tensor in the PE phase that appears when the friction between layers is null (i.e. ${}^p T_{ab} = 0$, so that ${}^p S_{0ab} = d_{kab}{}^p E_k$ by (6.8)), and ${}^p S_{ab}$ and ${}^m S_{ab}$ are the strains in the PE and MS phases, respectively. The coupling parameter consequently defines the ratio between the induced strains in the PE and MS layers. For an ideal interface we then have $k_c = 1$,

whereas for an interface without any friction between layers (i.e. without mechanical coupling between them) we get $k_c = 0$. The boundary conditions for the strain components on the lateral surfaces of the composite are therefore [72]:

$${}^pS_{ab} = k_c {}^mS_{ab} + (1 - k_c) {}^pS_{a0}. \quad (6.14)$$

It is further assumed that the interface is perfectly electromechanically bound. Consequently, the in-plane electric and magnetic fields will be continuous along the composite, the change in the normal displacement fields across the interfaces will be equal to the surface charge density (σ) and the normal magnetic induction will be continuous [43, 107]:

$${}^pE_1 = {}^mE_1, {}^pE_2 = {}^mE_2, {}^pD_3 - {}^mD_3 = \sigma; \quad (6.15)$$

$${}^pH_1 = {}^mH_1, {}^pH_2 = {}^mH_2, {}^pB_3 = {}^mB_3. \quad (6.16)$$

We now seek to find the expression for the direct ME voltage coefficient given by $\alpha_{Eij} = \partial^p E_i / \partial^m H_j$, or the electric field induced in the PE when the MS layers are subjected to an external magnetic field. By substitution of the constitutive equations (6.8) and (6.11) into (6.14) we get:

$${}^p s_{abkl}^E {}^p T_{kl} + k_c d_{km} {}^p E_k = k_c {}^m s_{abkl}^E {}^m T_{kl} + k_c ({}^m S_{0ab}(\mathbf{H}_0) + q_{kab}(\mathbf{H}_0) {}^m H_k) \quad (6.17)$$

Now adding the stress boundary conditions (6.12) and (6.13) to this expression and converting its parameters to the Voigt notation yields:

$$s_{mn} {}^p T_n + k_c d_{km} {}^p E_k = k_c ({}^m S_{0m}(\mathbf{H}_0) + q_{km}(\mathbf{H}_0) {}^m H_k), \text{ for } m, n = 1, 2 \text{ and } 6, \quad (6.18)$$

where $s_{mn} = {}^p s_{mn}^E + k_c f^m s_{mn}^E$ is an effective compliance and f is the ratio between the volume fractions of the PE and MS phases (${}^p v / {}^m v$). The rank-three square s_{mn} matrix in this expression can thus be inverted in order to write the PE stress ${}^p T_n$ explicitly as a function of the electric and magnetic fields. Subsequently, substituting this stress in the PE constitutive equation (6.7) and taking into account the elastic boundary conditions (6.12) we arrive at (in Voigt's notation):

$$\begin{aligned} {}^p D_k &= (\varepsilon_{kl}^T - k_c d_{km} s_{mn}^{-1} d_{ln}) {}^p E_l + k_c d_{km} s_{mn}^{-1} ({}^m S_{0n}(\mathbf{H}_0) + q_{jn}(\mathbf{H}_0) {}^m H_j), \text{ for } m, n \\ &= 1, 2 \text{ and } 6, \end{aligned} \quad (6.19)$$

where s_{mn}^{-1} is the inverse of the s_{mn} effective compliance matrix. Taking now into account that the magnetic layers consist of the electrically conductive Metglas alloy, the electric and displacement fields (${}^m D_i = \varepsilon_0 {}^m E_i$) in this layer should be approximately null and its top and bottom surfaces equipotential. Therefore one has [43, 107]:

$${}^m E_1 = {}^m E_2 = {}^m D_3 = 0 \quad (6.20)$$

By a substitution of the above relations in (6.15) one gets the additional conditions:

$${}^p E_1 = {}^p E_2 = 0; {}^p D_3 = \sigma. \quad (6.21)$$

Replacing this conditions in (6.19) one can finally write the ${}^p D_3$ component of the dielectric displacement as a function of the ${}^p E_3$ electric field and the magnetic fields in the MS layer:

$${}^p D_3 = (\epsilon_{33}^T - k_c d_{3m} s_{mn}^{-1} d_{3n}) {}^p E_3 + k_c d_{3m} s_{mn}^{-1} ({}^m S_{0n}(\mathbf{H}_0) + q_{jn}(\mathbf{H}_0) {}^m H_j), \text{ for } m, n = 1, 2 \text{ and } 6. \quad (6.22)$$

Supposing a magnetic field ${}^m H_k$ is applied to the composite along one of the three possible directions $k = 1, 2$ or 3 , one can therefore rearrange the expression above in order to obtain the variable ${}^p E_3$ explicitly as a linear function of this field as well as the ${}^p D_3$ field. Starting by considering an open circuit situation ($I = \int_{Area} {}^p \dot{D}_3 dA = 0$, where I is the current in the Z direction), in which ${}^p D_3$ equals an initial constant surface charge σ , as shown in (6.16), which we assume to be null (${}^p D_3 = 0$), and differentiating ${}^p E_3$ with respect to ${}^m H_k$, one finally arrives at the desired direct ME voltage coefficient. From this it follows that for $\mathbf{H} \rightarrow \mathbf{H}_0$ the general ME voltage coefficient can be written as a function of this field by the compact expression:

$$\alpha_{E3k}(\mathbf{H}) = \frac{\partial {}^p E_3}{\partial {}^m H_k}(\mathbf{H}) = \frac{-k_c d_{3m} s_{mn}^{-1} q_{kn}(\mathbf{H})}{\epsilon_{33}^T - k_c d_{3m} s_{mn}^{-1} d_{3n}}. \quad (6.23)$$

In the special case of a uniaxial PE (such as PZT ceramic with ∞m symmetry) which has only 2, 3 and 5 independent dielectric, PE and elastic constants, respectively, and a MS material, such as Metglas, with a normal orientation (∞m symmetry), this yields the result [36, 43]:

$$(\mathbf{H}) = \frac{\partial {}^p E_3}{\partial {}^m H_k}(\mathbf{H}) = \frac{-k_c d_{31} (q_{k1}(\mathbf{H}) + q_{k1}(\mathbf{H}))}{\epsilon_{33}^T [({}^p s_{11}^E + {}^p s_{12}^E) + k_c f ({}^m s_{11}^E + {}^m s_{12}^E)] - 2k_c d_{31}^2}, \quad (6.24)$$

which shows the tendency of the direct ME effect to be larger in composites containing PE phases with a large transverse piezocoefficient (d_{31}), small out-of-plane dielectric permittivity (ϵ_{33}^T) and small longitudinal and transverse compliance or flexibility (${}^p s_{11}^E + {}^p s_{12}^E$). Additionally, the MS phase should have large longitudinal and transverse piezomagnetic coefficients ($q_{k1}(\mathbf{H}) + q_{k2}(\mathbf{H})$) and small compliances (${}^m s_{11}^E + {}^m s_{12}^E$). The curves of this ME coefficient as a function of

the external magnetic field are known to follow those of the piezomagnetic coefficients [108]. The ME coefficient is thus proportional to the first derivative of the magnetostriction curve, increasing with the H field up to a given point, where the derivative of the magnetostriction is maximum, and decreasing progressively to zero afterwards, because the strain of the magnetic phase eventually saturates. Consequently, the piezomagnetic coefficients presented in literature often correspond to their maximum values for a given magnetic field, and the ME coefficients estimated by solving (6.23) will then correspond to the maximal expected coefficients for this field. Expression (6.24) additionally shows that, in order to maximize the ME effect, it is extremely important to obtain a good mechanical coupling between phases (i.e. a large k_c), thus guarantying an efficient transference of strain between them. Also, the thickness ratio between the PE and the MS layers should be as small as possible (i.e. small f), thus maximizing the in-plane tensile stress pT_n applied to the PE phase by the MS phase in the direction of the applied magnetic field, as seen by (6.18), while at the same time nullifying the compressive stress mT_n felt by the MS phase, as seen by (6.13). However, since the voltage measured in any real detection circuit associated with some input noise is proportional to the thickness of the PE layer, the maximal signal-to-noise ratio should be observed for a finite PE thickness. On the other hand, minimizing f by infinitely increasing the thickness of the MS layers would lead to unpractically large samples, so that some compromise has to be achieved for any given application.

The model shown in this part also permits the estimation of the quasi-static charge ME coefficient through a simple change in the electrical boundary conditions. For this case we consider a short-circuited composite ($V = -\int_{p_t}^p E_3 dZ = 0$, where V is the voltage developed across the PE) in such a way that we have ${}^pE_3 = 0$ instead of ${}^pD_3 = 0$ in (6.21). Subsequently (6.22) is differentiated in relation to mH_k thus yielding:

$$\alpha_{Q3k}(\mathbf{H}) = \frac{\partial^p D_3}{\partial^m H_k}(\mathbf{H}) = k_c d_{3m} s_{mn}^{-1} q_{kn}(\mathbf{H}). \quad (6.25)$$

Comparing the general (6.23) and (6.25), one notes that both the charge and voltage coefficients can be directly related by the expression $\alpha_{Q3k}(\mathbf{H}) = -(\epsilon_{33}^T - k_c d_{3m} s_{mn}^{-1} d_{3n}) \alpha_{E3k}(\mathbf{H})$, where $C = (\epsilon_{33}^T - k_c d_{3m} s_{mn}^{-1} d_{3n}) A / p_t$ represents the low frequency capacitance of the composite as it will be shown later. This capacitance tends therefore to decrease with increasing k_c (better coupling between layers) and decreasing f (thicker MS layers). For the case of uniaxial PE and MS materials, expression (6.25) is simplified to:

$$\alpha_{Q3k}(\mathbf{H}) = \frac{\partial^p D_3}{\partial^m H_k}(\mathbf{H}) = \frac{k_c d_{31} (q_{k1}(\mathbf{H}) + q_{k2}(\mathbf{H}))}{(p s_{11}^E + p s_{12}^E) + k_c f (m s_{11}^E + m s_{12}^E)} \quad (6.26)$$

which shows that, when compared to the α_{E3k} coefficient in (6.24), the charge coefficient is generally associated with a change of sign and no longer depends on

the dielectric permittivity ϵ_{33}^T of the PE. For the rest, all of the observations made before remain valid.

As mentioned before, up to this point the demagnetization effects on the MS layers have been neglected. For the special case of uniformly magnetized ellipsoids (with magnetization M_j) subjected to an uniform external magnetic field H'_k , the uniform field developed inside the material H_k can be given by $H_k = H'_k - N_{kj}M_j$, where N_{kj} is a demagnetization factor which depends on the shape of the ellipsoid [112]. In the case of an infinite plane with a normal pointing in the Z direction this demagnetization factor is given by $N_{33} = 1$ and $N_{kj} = 0$ otherwise [112]. Therefore, for thin enough MS layers the demagnetization fields can be neglected for H'_k applied in the X or Y directions (i.e. $H'_k = H_k$). However, in the case of thick MS phases, such that $N_{aa} \neq 0$, or the ME longitudinal effect where $H_3 \neq 0$, this effect can become quite substantial. The ME coefficients given by (6.23)–(6.26) can be corrected to take into account this effect. To do this, one starts by writing the external magnetic field H'_k as a function of the internal magnetic field H_k . Taking the demagnetization equation for some N_{kj} and making the substitution ${}^mM_j = {}^mB_j/\mu_0 - {}^mH_j$, one obtains ${}^mH'_k$ as a function of mH_j and the magnetic induction mB_j given by (6.10). Subsequently, through a series of substitutions involving (6.12), (6.13) and (6.18) one arrives at the final result:

$${}^mH'_k = \overline{H_{0k}}(\mathbf{H}_0) + \overline{\mu_{kl}}(\mathbf{H}_0) {}^mH_l + \overline{\alpha_{Qk3}}(\mathbf{H}_0) {}^pE_3, \quad (6.27)$$

where $\overline{H_{0k}}(\mathbf{H}_0) = (N_{kj}/\mu_0)({}^mB_{0j}(\mathbf{H}_0) - k_c f q_{jm}(\mathbf{H}_0) s_{mn}^{-1} {}^mS_{0n}(\mathbf{H}_0))$, $\overline{\alpha_{Qk3}}(\mathbf{H}_0) = (N_{kj}/\mu_0) k_c f q_{jm}(\mathbf{H}_0) s_{mn}^{-1} d_{3n}$, $\overline{\mu_{kl}}(\mathbf{H}_0) = \delta_{kl} - N_{kl} + \mu_{kl}(\mathbf{H}_0) - k_c f q_{km}(\mathbf{H}_0) s_{mn}^{-1} q_m(\mathbf{H}_0)$ and pE_3 is related to mH_j and pD_3 through (6.22). The corrected ME voltage coefficients written as a function of the known external magnetic fields $\mathbf{H}' \rightarrow \mathbf{H}'_0$ can therefore be given as $\alpha'_{E3k}(\mathbf{H}') = \partial^p E_3 / \partial {}^m H'_k(\mathbf{H}') = \partial^p E_3 / \partial {}^m H_j(\mathbf{H}(\mathbf{H}')) \cdot \partial {}^m H_j / \partial {}^m H'_k(\mathbf{H}')$, which reduces to:

$$\alpha'_{E3k}(\mathbf{H}') = \alpha_{E3j}(\mathbf{H}(\mathbf{H}')) \left[\overline{\mu_{jl}}^{-1}(\mathbf{H}(\mathbf{H}')) \left[\delta_{lk} - \overline{\alpha_{Ql3}}(\mathbf{H}(\mathbf{H}')) \alpha_{E3k}(\mathbf{H}(\mathbf{H}')) \right] \right] \quad (6.28)$$

where $\overline{\mu_{jl}}^{-1}(\mathbf{H}(\mathbf{H}'))$ is the inverse of the $\overline{\mu_{kl}}(\mathbf{H}_0)$ function, $\alpha_{E3j}(\mathbf{H}(\mathbf{H}'))$ is given by (6.23) and $\mathbf{H}(\mathbf{H}')$ is determined by solving the implicit expression (6.27). In summary, the maximum ME effects of composites subjected to demagnetization effects tend to be smaller and appear at larger applied magnetic fields [6].

The aforementioned ME coefficients were defined for ideal open-circuit or short-circuit conditions. However, in experimentation the ME composites are operated under non-ideal conditions in which case the parameters of the external measuring circuits have to be taken into account. Therefore it is useful to model the composites as equivalent electrical circuits. In this regard, assuming harmonic fields

of the type ${}^m H_k = {}^m H_{0k} + \delta H_k e^{j\omega t}$, where ${}^m H_{0k}$ is a bias field, δH_k a complex amplitude, j the imaginary unit, ω the angular frequency and t the time, and differentiating (6.22) with respect to time and integrating it over the volume of the composite (i.e. $\int_{p_t Area} \int \rho \dot{D}_3 dAdZ$) we can derive the relation:

$$\delta V_3 = (-\alpha_{E3k} ({}^m H_{0k})^{p_t}) \delta H_k - (1/j\omega C) \delta I_3, \quad (6.29)$$

where $\delta V_3 = -\int_{p_t} \delta^\rho E_3 dZ$ is the AC voltage measured between the top and bottom of the composite and $\delta I_3 = j\omega \int_{Area} \delta^\rho D_3 dA$ is the AC current flowing through it in the Z direction. This expression thus shows that the composite can be modeled as a Thévenin equivalent circuit consisting of an equivalent voltage source of $\delta V_{Th}(\mathbf{H}) = (-\alpha_{E3k} ({}^m H_{0k})^{p_t}) \delta H_k$ connected in series with an equivalent impedance given by $Z_{Th} = 1/j\omega C$ which represents a capacitor with capacitance $C = (\epsilon_{33}^T - k_c d_{3m} s_{mn}^{-1} d_{3n}) A / p_t$. Equivalently, the composite can also be modeled as a Norton equivalent circuit composed of a current source of $\delta I_{No}(\mathbf{H}) = (j\omega \alpha_{Q3k} ({}^m H_{0k}) A) \delta H_k$ connected in parallel with the same impedance. More precisely, by taking into account the important effects of dielectric dispersion ($\epsilon_{33}^T(\omega)$), dielectric losses ($\epsilon_{33}^{T''}(\omega)$) and conductivity (σ) of the PE through the introduction of the complex dielectric coefficient $\epsilon_{33}^T(\omega) = \epsilon_{33}^{T'}(\omega) - j\epsilon_{33}^{T''}(\omega) + \sigma/j\omega = \epsilon_{33}^{T'}(\omega) - j\epsilon_{33}^{T''}(\omega) \tan(\delta)$, where $\omega \epsilon_{33}^{T''}(\omega) \tan(\delta)$ is the so called dissipation factor, the equivalent impedance of the composite can be given by $Z_{Th} = 1/(1/R' + j\omega C')$ which corresponds to a capacitor with $C' = (\epsilon_{33}^{T'}(\omega) - k_c d_{3m} s_{mn}^{-1} d_{3n}) A / p_t$ connected in parallel with a resistor with $R' = p_t / A \omega \epsilon_{33}^{T''}(\omega) \tan(\delta)$. In conclusion, when measuring for example the ME voltage coefficient, the finite input impedance of the measuring circuit should always be taken into account. Assuming e.g. an input impedance of $Z_{in} = 1/(1/R_{in} + j\omega C_{in})$ as in the case of a lock-in amplifier, the measured voltage in such a device as a function of the magnetic fields will be given by $\delta V_{in} = (Z_{in} / (Z_{Th} + Z_{in})) \delta V_{Th}(\mathbf{H})$. Thus, the circuit will generally behave as a high-pass filter with a small input amplitude $|\delta V_{in}| = (R_{in} / (R' + R_{in})) |\delta V_{Th}(\mathbf{H})|$ being measured at zero frequency (because R' usually takes a much larger value than R_{in} in a lock-in amplifier) and a larger input amplitude $|\delta V_{in}| = (C' / (C' + C_{in})) |\delta V_{Th}(\mathbf{H})|$ measured at large frequencies (because C_{in} is normally much smaller than C'). Another important application of this circuit model is in the development of sensitive low-noise magnetic field sensors based on the ME effect [47, 49].

ME composites comprising PE single crystals have been the subject of a few recent studies including PMN-PT [48, 113–115], PZN-PT [116], barium titanate (BaTiO_3) [117], lithium niobate (LiNbO_3) [113, 118], gallium phosphate (GaPO_4) [119], quartz (SiO_2) [120], aluminum nitride (AlN) [94], zinc oxide (ZnO) [121], langatate ($\text{La}_3\text{Ga}_{5.5}\text{Ta}_{0.5}\text{O}_{14}$, LGT) [122, 123] and langasite ($\text{La}_3\text{Ga}_{5.5}\text{SiO}_{14}$, LGS)

[123]. These have promised further enhancement of the ME coupling. Since single crystals are highly anisotropic, their electric and elastic properties sensitively depend on their crystallographic orientation. Therefore, the optimization of the orientation could lead to greatly enhanced ME coefficients in composites. To study this dependency of the ME coupling on the crystal orientation, we have to subject the material tensors to a passive transformation of coordinates. Equations (6.6)–(6.29) contain the material coefficients and fields defined in the laminate XYZ frame of Fig. 6.1a. However, the material properties are usually described in the crystallographic xyz frame, and that is why we have to transform them to the laminate frame before applying the equations. To do so, the rotation matrix a_{ij} is introduced, where the Euler angles $Z_1X_2Z_3$ scheme (see Fig. 6.1b) is employed [111]:

$$\mathbf{a} = \begin{bmatrix} \cos(\gamma) \cos(\alpha) - \cos(\beta) \sin(\alpha) \sin(\gamma) & \cos(\gamma) \sin(\alpha) + \cos(\beta) \cos(\alpha) \sin(\gamma) & \sin(\gamma) \sin(\beta) \\ -\sin(\gamma) \cos(\alpha) - \cos(\beta) \sin(\alpha) \cos(\gamma) & -\sin(\gamma) \sin(\alpha) + \cos(\beta) \cos(\alpha) \cos(\gamma) & \cos(\gamma) \sin(\beta) \\ \sin(\beta) \sin(\alpha) & -\sin(\beta) \cos(\alpha) & \cos(\beta) \end{bmatrix} \quad (6.30)$$

This matrix describes a sequence of three elemental rotations, the first about the Z axis by an angle α , the second about the X axis by an angle β , and the third again about the Z axis by an angle γ . In this case, after applying the rotation matrix to the crystal, the angles α and β will identify the vector normal to the plane of the laminate, and the angle γ will determine the orientation of the side faces of the laminate in this plane (and consequently the direction of the applied in-plane magnetic fields). Upon changing the frame of reference, the material parameters follow the specific tensor transformation rules which also define the second-, third- and fourth-rank tensors [104]:

$$\varepsilon_{ij} = a_{im} a_{jn} \varepsilon'_{mn}, \quad d_{ijk} = a_{im} a_{jn} a_{ko} d'_{mno}, \quad s_{ijkl} = a_{im} a_{jn} a_{ko} a_{lp} s'_{mnop} \quad (6.31)$$

where the constants with an apostrophe denote the material properties in the initial crystallographic frame, and those without apostrophe—the properties in the new frame of reference described by the transformation \mathbf{a} .

6.2.3 Estimation of the Quasi-Static Transversal ME Voltage Coefficients in Magnetostrictive/Piezocrystalline/Magnetostrictive Tri-Layers

We are now in possession of all the tools we need in order to estimate and optimize the transversal ME response (α_{E3i} , with $i = 1$ or 2) in a series of tri-layered composites containing two layers of Metglas bonded to a PE single crystal of some sort. To do so, we create a fine grid of Euler angles in steps of 1° and subsequently analyze the estimations for these angles. The composites we investigated had the

shape of a square plate like the one shown in Fig. 6.1a, where we considered $10 \times 10 \text{ mm}^2$ sheets of Metglas with $29 \text{ }\mu\text{m}$ of thickness bonded to opposite sides of a $10 \times 10 \text{ mm}^2$ PE crystal with a thickness of 0.5 mm . A perfect coupling between interfaces was assumed ($k_c = 1$). In a traction-free Metglas layer a maximum q_{11} value of ca. 4 ppm/Oe and q_{12} of ca. -1.7 ppm/Oe are attained at a bias field of ca. 10 Oe [124–127]. These were therefore taken as our piezomagnetic coefficients. All of the dielectric, piezoelectric, piezomagnetic (for Metglas [124–127]) and elastic material parameters needed for these calculations were obtained from the literature. The lead-free piezoelectrics studied here thus have included: LiNbO_3 [57, 128], $\alpha\text{-GaPO}_4$ [58, 59], $\alpha\text{-quartz}$ [129, 130], langatate [131, 132], langasite [133, 134], AlN [135, 136], LiTaO_3 [137–139] and BaTiO_3 [55, 56], and also the lead-based ones, viz., PZT-2 [140], PMN-33 %PT ([111] poled) [141], PMN-30 %PT ([011] poled) [62], PMN-33 %PT ([001] poled) [142], PZN-9 %PT ([011] poled) [143] and PZN-8 %PT ([001] poled) [144].

The results obtained by solving (6.23) are summarized in Table 6.3 which shows the maximum expected direct ME coefficients for each composite and respective optimal crystallographic orientations of the PE phase. From these estimations we confirmed the possibility of generating large quasi-static ME effects in ME composites comprising lead-free PE single crystals. Here, coefficients as large as $35.6 \text{ V}/(\text{cm}\cdot\text{Oe})$ are expected. These ME effects are particularly attractive for the tri-layers comprising LiNbO_3 , GaPO_4 , quartz, PMN-33 %PT ([111] poled) and PZN-9 %PT ([011] poled) originating from a particularly good combination of relatively large PE coefficients and low dielectric constants. Also, because the maximum expected ME effects are of the same order of magnitude in both lead-based and lead-free PEs, such exclusive features as chemical stability, linear piezoelectricity and high Curie temperature (in the range of $570\text{--}1475 \text{ }^\circ\text{C}$) open up a real perspective to use these lead-free PE-based magnetoelectric tri-layers in practical applications.

The selection of crystals with an appropriate cut is a very important step in the development of ME composites. The engineering of these cuts should in principle allow one to develop materials with specific anisotropic properties desired for each type of practical application. Large ME effects are particularly important in applications requiring enhanced efficiencies and sensitivities. Figure 6.2 thus shows the maximum absolute transversal ME coefficients (in the range of all spanned γ angles) estimated as a function of the α and β angles for all considered tri-layers. In the figures we notice the great sensitivity of the ME effect to the orientation of the piezocrystal. The shape of the figures depends on the point group symmetry of the PE mainly through the term $|g_{31} - g_{32}|$ which indicates the difference between PE voltage coefficients ($g_{ij} = -\partial E_i / \partial T_j = \varepsilon_{ik}^{-1} d_{kj}$) for stresses directed along both lateral surfaces of the crystal, since the elastic term varies much less with the orientation of the crystal.

We note at this point that, alongside the dispersion and losses of the material's properties not taken into account, a much more important limitation of the model is the fact that the piezomagnetic coefficients of Metglas are also strongly dependent on the bias magnetic fields and stress tensors. A more complex model for the soft

Table 6.3 Estimation of the maximum expected transversal direct ME voltage coefficients for a series of $10 \times 10 \text{ mm}^2$ ME tri-layered composites composed of two 29 μm thick layers of MeGlas and one central 0.5 mm thick PE crystal of some kind

PE crystal	LiNbO ₃	α -GaPO ₄	α -Quartz	Langatate (LGT)	Langasite (LGS)	AlN	LiTaO ₃	BaTiO ₃
Maximum $ \alpha_{E_{3a}} $ (V/(cm·Oe))	27.24	35.62	23.77	16.68	16.59	13.06	11.40	10.74
Z-cut crystal $\alpha_{E_{3a}}$ (V/(cm·Oe))	1.23	0	0	0	0	8.16	2.89	10.74
Optimal orientation	α	60	30	30	30	90	0	60
		120	150	210	150	210	120	180
		240	330	270	270	330	240	300
	β	39	141	90	90	90	60	45
	90	90	168	11	156	24	90	135
								90
								180
Crystal cut	(ZX) 39°	(XY) 12°	(XY) 11°	(XY) 24°	(XY) 20°	(ZX) 60°	(ZX) 45°	Z
PE crystal	PZT-2		PMN-33 %PT ((111) poled)	PMN-30 %PT ((011) poled)	PMN-33 %PT ((001) poled)	PZN-9 %PT ((011) poled)	PZN-8 %PT ((001) poled)	
Maximum $ \alpha_{E_{3a}} $ (V/(cm·Oe))	7.47	5.78	27.11	12.50	10.80	23.04	8.30	
Z-cut crystal $\alpha_{E_{3a}}$ (V/(cm·Oe))	5.41			12.50	6.29	23.04	7.66	
Optimal orientation	α	0-360	0-360	0-360	0-360	45	0-360	45
			60	180	135	135	180	135
			120	240	225	225	240	225
			300	300	315	315	300	315
	β	37	143	42	138	64	180	38
		90	90	90	90	90	90	90
Crystal cut	(ZX) 37°	(ZX) 42°	Z	(ZX) 45°/64°	Z	(ZX) 45°/38°	Z	

The optimal crystallographic orientations and corresponding crystal cuts according to the IEEE standard [54] are also presented. Here, the optimal orientations are given as a set of Euler angles (α , β and γ in deg.), where the first column indicates the possible combinations of angles (equivalent by symmetry) corresponding to the same absolute maximum positive ME effect, whereas the second column gives the combination of angles for the same absolute maximum but negative ME effect (i.e., with an inversion in the sign of the ME coupling coefficient). The frame of reference in each case corresponds to the crystallographic frame except in PZT, PMN-PT and PZN-PT, where it corresponds to their respective poled multidomain frames with the Z axis directed along their poling directions

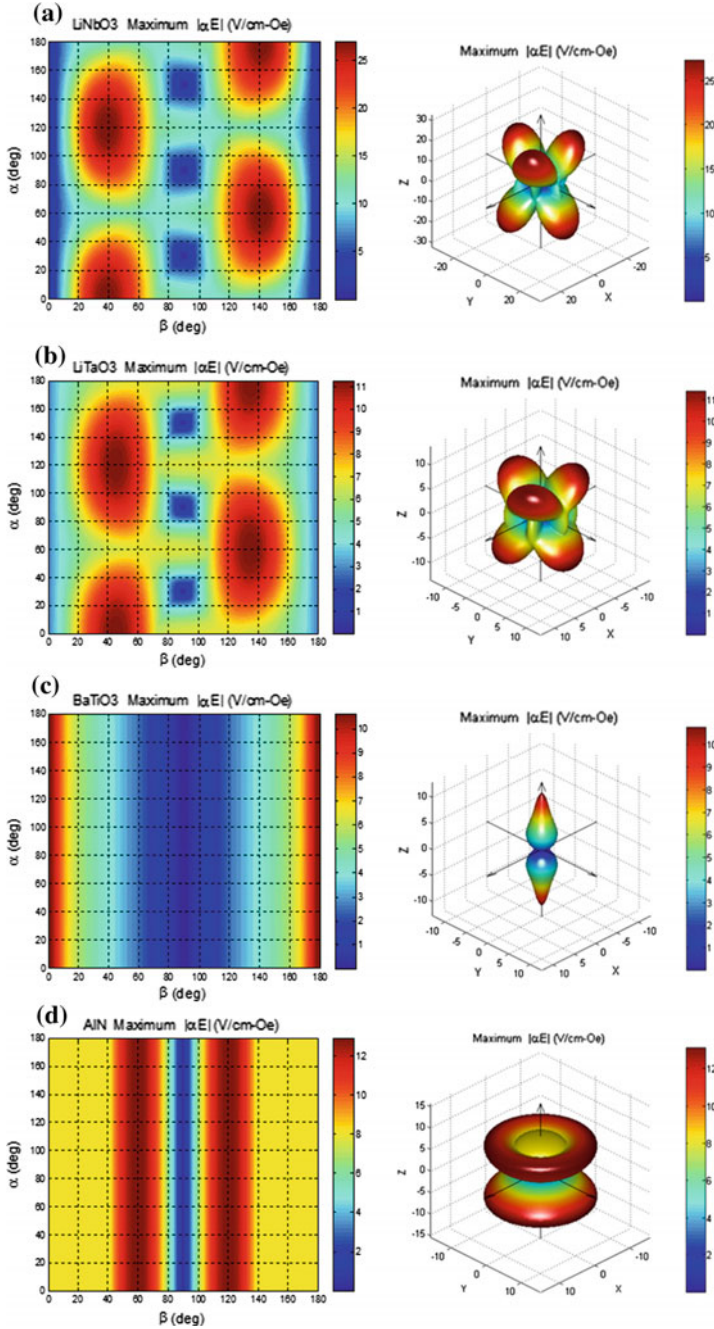


Fig. 6.2 Contour plots and $|\alpha_{E31}|$ representation surfaces depicting the maximum estimated absolute values of the transversal ME voltage coefficient α_{E31} (across $0 < \gamma < 180^\circ$) as a function of the crystal orientation (α and β angles) for the tri-layered ME composites of Metglas/PE/Metglas, where the PE phase is a single crystal of: **a** LiNbO_3 ; **b** LiTaO_3 ; **c** BaTiO_3 ; **d** AlN ; **e** α -quartz; **f** α - GaPO_4 ; **g** langatate; **h** langasite; **i** PZT-2; **j** PMN-33 %PT ([111] poled); **k** PMN-30 %PT ([011] poled); **l** PMN-33 %PT ([001] poled); **m** PZN-9 %PT ([011] poled) and **n** PZN-8 %PT ([001] poled)

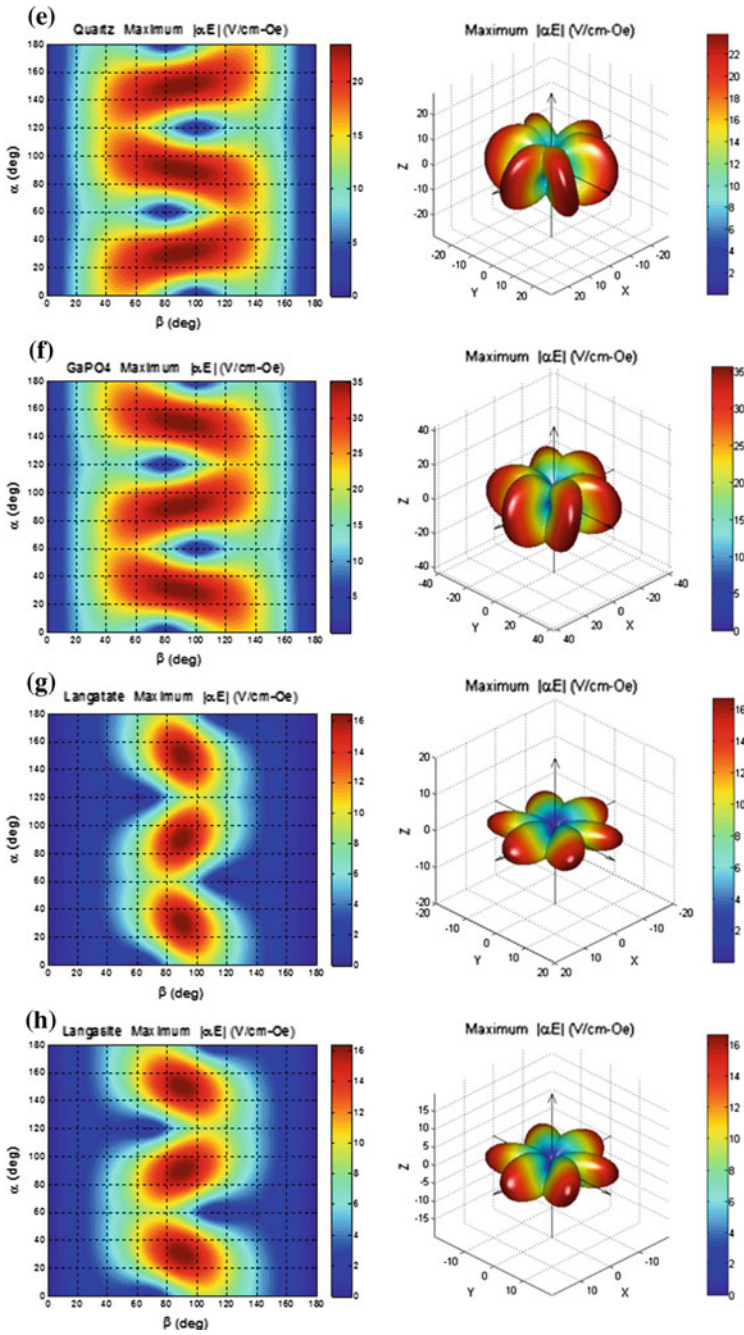


Fig. 6.2 (continued)

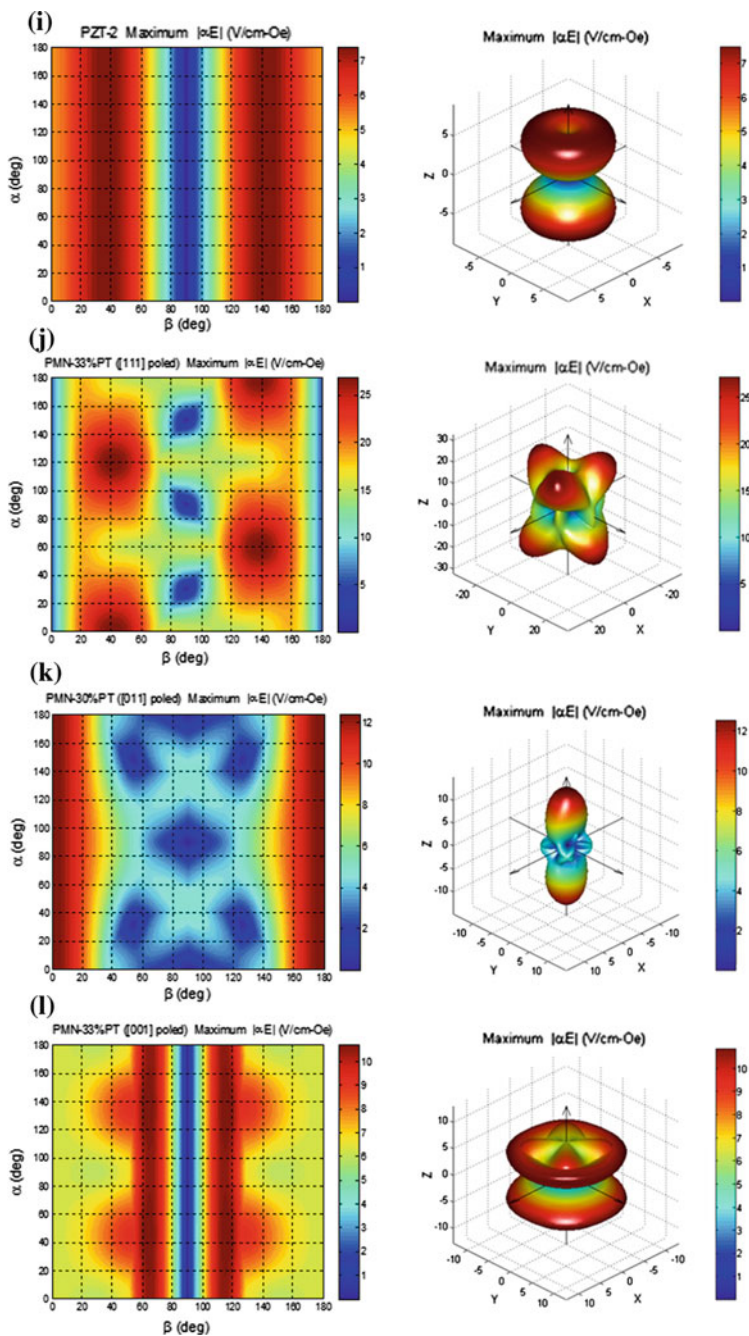


Fig. 6.2 (continued)

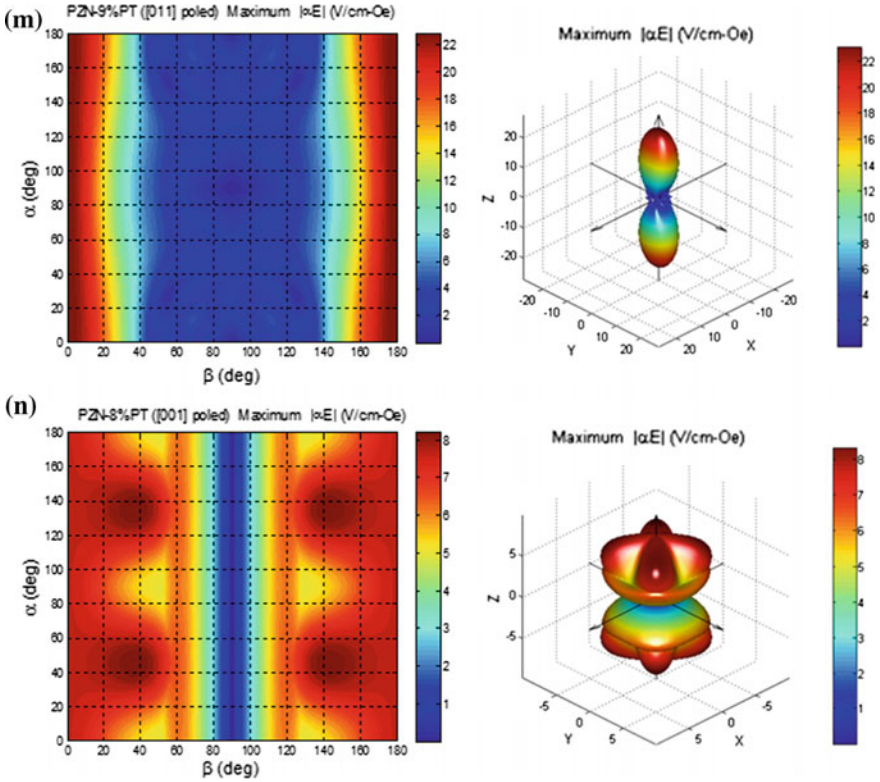


Fig. 6.2 (continued)

MS phase shows for example that the large compressive pre-stress produced by the PE substrate in the MS sheets tends to decrease the maximum value of q_{kn} and at the same time increase the bias field at which it is attained [145]. Therefore, the maximum ME coefficients predicted in this part should be somewhat overestimated. Nonetheless, the relation between ME coefficients obtained for the composites with different PE crystals still remains valid. Furthermore, we point out that the thickness ratio between the MS and PE layers in the composites was not optimized for a maximum ME response. Thicker MS layers are expected to produce a larger effective strain on the PE crystal and thus increase the amplitude of the ME effect by up to one order of magnitude. In this calculations, 29 μm thick layers of Metglas were used because, in practice, some peculiarities associated with the fabrication of these alloys (i.e. a melt spinning rapid solidification process) restricts their thickness to just a few of tens of μm . Also, commercial PE crystals are generally found with thicknesses no smaller than 0.2 mm.

In the next paragraphs we are going to discuss the results of the calculations in greater detail. Starting with the case of the LiNbO_3 crystal, which belongs to the trigonal $3m$ symmetry point group, we see that the estimated ME coefficient could

be as large as 27.24 V/(cm·Oe) for a crystal with a (*ZXl*) 39°-cut ($\alpha = 0^\circ$, $\beta = 39^\circ$ and $\gamma = 90^\circ$), commercially commonly referred to as 129°Y-cut, and five other cuts equivalent by symmetry. We also see that this effect stays within 90 % of its maximum value for cut deviations, in relation to its optimal orientation, of approximately $\Delta\alpha = \pm 20^\circ$ and $\Delta\beta = \pm 10^\circ$. LiTaO₃ has the same symmetry as LiNbO₃, but we calculated in this case an expected coefficient of 11.40 V/(cm·Oe), being about 3 times smaller than that in the former material. This is mainly because of its characteristically smaller PE coefficients (especially its d_{15} and d_{22} components), as well as comparable dielectric constants. The maximum effect should be observed in a (*ZXl*) 45°-cut crystal ($\alpha = 0^\circ$, $\beta = 45^\circ$ and $\gamma = 90^\circ$) and also other five equivalent cuts. This coefficient decreases by less than 10 % for cut deviations of about $\Delta\alpha = \pm 25^\circ$ and $\Delta\beta = \pm 10^\circ$. BaTiO₃ single crystals belong to the tetragonal *4mm* point group and have much larger PE and dielectric coefficients than LiNbO₃. The largest expected ME coefficient here is just of 10.74 V/(cm·Oe) and is only observed in the Z-cut crystal, decaying very rapidly as we move away from this optimal orientation. AlN piezocrystals exhibit a hexagonal *6mm* symmetry and relatively small dielectric and PE coefficients. The maximum coefficient for a composite containing this phase was calculated as 13.06 V/(cm·Oe) for the (*ZXl*) 60°-cut ($0^\circ \leq \alpha < 360^\circ$, $\beta = 60^\circ$ and $\gamma = 90^\circ$) and (*ZXl*) 120°-cut crystals. As in BaTiO₃, this effect is axially symmetric and stays within 90 % of its maximum value for cut deviations of approximately $\Delta\beta = \pm 10^\circ$.

The α -quartz and α -GaPO₄ PE crystals are another class of lead-free piezoelectrics which, like LiNbO₃, exhibit relatively large ratios between PE and dielectric constants. They both belong to the trigonal 32 point group. The most noticeable differences between them are related to the PE coefficients, which are approximately twice as large for the case of GaPO₄, as well as the dielectric coefficients which are about 20 % larger in GaPO₄ as compared to quartz. Even though they have some of the smallest piezoconstants among the piezocrystals studied in this chapter, their dielectric permittivities are also comparatively small, which therefore gives rise to large PE/dielectric ratios and consequently opens the possibility for large ME responses in the composites. Indeed, following the model described above we calculated maximum ME coefficients of 35.62 and 23.77 V/(cm·Oe) for the GaPO₄ and quartz crystals, respectively. These values are quite high and may be observed in (*XYt*) 12°-cut ($\alpha = 90^\circ$, $\beta = 90^\circ$ and $\gamma = 12^\circ$) crystals of GaPO₄ and in (*XYt*) 11°-cut ($\alpha = 90^\circ$, $\beta = 90^\circ$ and $\gamma = 11^\circ$) crystals of quartz, as well as in other five cut directions equivalent by symmetry. We also note that these cuts are quite near the X-cut direction. In this case, the ME coefficient decreases by less than 10 % for cut deviations from the maximum direction of about $\Delta\alpha = \pm 10^\circ$ and $\Delta\beta = \pm 25^\circ$.

Langatate and langasite are other two piezoelectrics belonging to the trigonal 32 point group. They are characterized by PE coefficients comparable to the ones of GaPO₄, but also exhibit considerably larger dielectric coefficients. Their maximum expected ME coefficients were calculated as 16.68 V/(cm·Oe) for an (*XYt*) 24°-cut crystal ($\alpha = 90^\circ$, $\beta = 90^\circ$ and $\gamma = 24^\circ$), in the case of langatate, and 16.59 V/(cm·Oe) for an (*XYt*) 20°-cut crystal ($\alpha = 90^\circ$, $\beta = 90^\circ$ and $\gamma = 20^\circ$), in the case of langasite.

Furthermore, the maximum ME effect is more sensitive to the cut angle in these two crystals. We observe that the effect stays within 90 % of its maximum value for cut deviations of just about $\Delta\alpha = \pm 10^\circ$ and $\Delta\beta = \pm 10^\circ$.

In the class of the lead-based piezoelectrics we start by looking at the PZT-2 uniaxial ceramic having an ∞mm symmetry. As we know, its PE and dielectric properties are quite distinguished. Still, the maximum direct ME coefficient of just about 7.47 V/(cm·Oe) was calculated for the (Z*Xl*) 37°-cut direction ($0^\circ \leq \alpha < 360^\circ$, $\beta = 37^\circ$ and $\gamma = 90^\circ$) and another equivalent direction. Even though this compound constitutes one of the piezoelectrics most commonly employed in practice, we note that its maximum expected ME response is the smallest among all piezo-crystals studied in this chapter. This fact underlines the importance of the dielectric properties of the materials employed in ME composites. Thus, we see that compounds with merely large PE coefficients do not necessarily yield large direct ME effects. We also observe that for this PZT-2 ceramic the maximum ME coefficient changes little for cut angles in the range $0^\circ \leq \beta < 60^\circ$ and $120^\circ \leq \beta < 180^\circ$. Therefore, common commercially available Z-cut ceramics still could exhibit a maximum 5.41 V/(cm·Oe) ME response.

PMN-PT crystals are a family of lead-based macrosymmetric multidomain engineered piezoelectrics. Here we studied the ME effect in composites featuring the following compositions: [111] poled PMN-33 %PT, [011] poled PMN-30 %PT and [001] poled PMN-33 %PT. The first compound has a trigonal $3m$ symmetry, while the second and third have an orthorhombic $mm2$ and tetragonal $4mm$ macrosymmetry, respectively. From a general point of view, the [011] poled crystal exhibits the largest dielectric coefficients, followed by the [001] poled and the [111] poled ones. The largest piezocoefficients in each crystal are $d_{15} = 4100$ pC/N, $d_{15} = 3262$ pC/N and $d_{33} = 2820$ pC/N in the [111], [011] and [001] poled compounds, respectively. In the calculations we identified a relatively large maximum direct ME coefficient of 27.11 V/(cm·Oe) in the [111] poled and (Z*Xl*) 42°-cut PMN-PT crystal ($\alpha = 0^\circ$, $\beta = 42^\circ$ and $\gamma = 90^\circ$), and five other equivalent directions, although this is just of 5.78 V/(cm·Oe) in the Z-cut crystal. The maximum coefficient decays by more than 10 % of its highest value for angle deviations larger than $\Delta\alpha = \pm 10^\circ$ and $\Delta\beta = \pm 10^\circ$ from the optimal orientation. In the [011] poled crystal, the largest expected value is of 12.50 V/(cm·Oe), and it is observed in the Z-cut crystal. This coefficient changes only slightly for $\Delta\beta = \pm 10^\circ$. In the [001] poled PMN-PT crystal the maximum is of 10.80 V/(cm·Oe) and should be attained in the crystal with a (Z*Xit*) 45°/64° complex cut ($\alpha = 45^\circ$, $\beta = 64^\circ$ and $\gamma = 90^\circ$), and seven other directions. The most common Z-cut could exhibit a ME response of up to 6.29 V/(cm·Oe). By symmetry considerations, an almost maximized ME effect could, nonetheless, be observed in the range of $60^\circ \leq \beta < 70^\circ$ and $110^\circ \leq \beta < 120^\circ$, for any α angle.

Finally, we also studied PZN-PT piezocrystals with engineered domain structures. Those where the [011] poled PZN-9 %PT, with an orthorhombic $mm2$ macrosymmetry, and the [001] poled PZN-8 %PT, with a tetragonal $4mm$ macrosymmetry. The first crystal has a large difference between transversal PE coefficients $|d_{31} - d_{32}| = 2181$ pC/N, which therefore explains its large calculated

maximum direct ME coefficient of 23.04 V/(cm·Oe) in the Z-cut crystal. As in the [011] poled PMN-PT, this coefficient changes only slightly for $\beta = \pm 10^\circ$. In the [001] poled PZN-8 %PT, the maximum effect was estimated as 8.30 V/(cm·Oe) for the (ZXtl) 45°/38°-cut ($\alpha = 45^\circ$, $\beta = 38^\circ$ and $\gamma = 0^\circ$), and seven other directions. In the Z-cut crystal, this decays just to 7.66 V/(cm·Oe). Mainly, the maximum coefficient decreases by less than 10 % of its largest value for cut deviations of approximately $\Delta\alpha = \pm 10^\circ$ and $\Delta\beta = \pm 10^\circ$.

In summary, using an averaging model based on the constitutive equations, we have predicted the possibility of producing large ME responses in tri-layered composites employing suitably cut PE crystals. Especially strong ME effects are expected for single crystals of LiNbO₃, α -GaPO₄, α -quartz, [111] poled PMN-33 %PT and [011] poled PZN-9 %PT. Even so, in practice the use of the first three in ME composites still remains largely unexplored.

6.3 Conclusions

A theoretical model of the anisotropic quasi-static direct ME effect in tri-layered composites of metglas and PE single crystals has been used in the quantitative estimation of the ME coupling as a function of the crystallographic orientation (i.e. PE cut plane). First, a description of the PE and linear MS (in the pseudo-piezomagnetic approximation) effects in terms of electric, magnetic and elastic material fields and constants has been given. An averaging quasi-static method was subsequently used together with specific boundary conditions in order to derive the relation between the material constants and the transversal (T-L) direct ME voltage (α_{E3a}) and charge coefficients (α_{Q3a}). The method consisted of the solution of the elastostatic and electrostatic equations taking into account the linear constitutive relations of the two phases. The properties of some common PE and MS materials (the latter with emphasis on the metglas alloy exhibiting giant MS) have been discussed, and their influence on the ME coupling has been explored. It has been demonstrated that large ME voltage coefficients tend to be favored by large transversal PE coefficients, transversal and longitudinal piezomagnetic coefficients and coupling constants as well as small out-of-plane dielectric and compliance constants and the volume ratio between the PE and MS phases. On the other hand, it has also been shown that the ME charge coefficients do not depend on the dielectric constants of the PEs and thus tend to be much larger in lead-based crystals with very large piezoelectric constants such as PMN-PT and PZN-PT. The effects of the demagnetization fields on the attenuation of the ME coefficients were briefly explored. A description of the ME composites as equivalent Thévenin/Norton circuits composed of a magnetically driven voltage/current source in series/parallel with a characteristic impedance of the composite has also been exposed.

After that, we used the quasi-static model for the calculation of the maximum expected direct transversal ME voltage coefficients in a series of tri-layered composites of the type Metglas/Piezocrystal/Metglas, as a function of the PE crystal

orientation. The PE single crystals studied in this chapter included lead-free lithium niobate, α -gallium phosphate, α -quartz, langatate, langasite, aluminum nitride, lithium tantalate and barium titanate, as well as the lead-based PZT-2, PMN-33 %PT ([111] poled), PMN-30 %PT ([011] poled), PMN-33 %PT ([001] poled), PZN-9 %PT ([011] poled) and PZN-8 %PT ([001] poled). The estimations revealed a strong dependence of the ME effects on the crystal orientation. They also supported the possibility of generating large quasi-static ME voltage coefficients in composites comprising lead-free PE single crystals through the optimization of the crystal orientation. These ME effects were found to be particularly attractive for the case of lithium niobate, α -gallium phosphate, quartz, [111]-poled PMN-33 %PT and [011]-poled PZN-9 %PT. The enhanced effects were found to originate from a particularly good combination of relatively large PE coefficients and low dielectric constants. We thus have revealed that the choice of crystals with an appropriate cut is a vital step in the development of ME composites valuable for practical applications.

Acknowledgments This work was developed in the scope of the projects I3N/FSCOSD (Ref. FCT UID/CTM/50025/2013), CICECO – Aveiro Institute of Materials – POCI-01-0145-FEDER-007679 (FCT Ref. UID/CTM/50011/2013), and RECI/FIS-NAN/0183/2012 (FCOMP-01-0124-FEDER-027494) financed by national funds through the FCT/MEC and when applicable cofinanced by FEDER under the PT2020 Partnership Agreement. J.V.V. and A.A.T. thank for the FCT grants SFRH/BD/89097/2012 and SFRH/BPD/74086/2010, respectively. N.A.S. acknowledges support by NUST “MISiS” through grant no. K3-2015-003.

References

1. P. Debye, Bemerkung zu einigen neuen Versuchen über einen magneto-elektrischen Richteffekt. *Z. Phys.* **36**(4), 300–301 (1926)
2. T.H. O’Dell, *The Electrodynamics of Continuous Media* (North-Holland, Amsterdam, 1970)
3. L.D. Landau, L.P. Pitaevskii, E. M. Lifshitz, *Electrodynamics of Continuous Media*. 2nd edn. vol. 8 (Course of Theoretical Physics), Butterworth-Heinemann (1984)
4. M. Fiebig, N.A. Spaldin, Current trends of the magnetoelectric effect. *Eur. Phys. J. B* **71**(3), 293–297 (2009)
5. W. Eerenstein, N.D. Mathur, J.F. Scott, Multiferroic and magnetoelectric materials. *Nature* **442**(7104), 759–765 (2006)
6. C.-W. Nan, M.I. Bichurin, S. Dong, D. Viehland, G. Srinivasan, Multiferroic magnetoelectric composites: historical perspective, status, and future directions. *J. Appl. Phys.* **103**(3), 031101–031135 (2008)
7. M. Fiebig, Revival of the magnetoelectric effect. *J. Phys. D Appl. Phys.* **38**(8), R123–R152 (2005)
8. S.-W. Cheong, M. Mostovoy, Multiferroics: a magnetic twist for ferroelectricity. *Nat. Mater.* **6**(1), 13–20 (2007)
9. R. Ramesh, N.A. Spaldin, Multiferroics: progress and prospects in thin films. *Nat. Mater.* **6**(1), 21–29 (2007).
10. R. Ramesh, Materials science: Emerging routes to multiferroics. *Nature* **461**(7268), 1218–1219 (2009)

11. N.A. Spaldin, M. Fiebig, The renaissance of magnetoelectric multiferroics. *Science* **309**(5733), 391–392 (2005)
12. M. Bichurin, D. Viehland, G. Srinivasan, Magnetoelectric interactions in ferromagnetic-piezoelectric layered structures: phenomena and devices. *J. Electroceram.* **19**(4), 243–250 (2007)
13. Y. Wang, J. Hu, Y. Lin, C.-W. Nan, Multiferroic magnetoelectric composite nanostructures. *NPG Asia Mater.* **2**(2), 61–68 (2010)
14. J. Zhai, Z. Xing, S. Dong, J. Li, D. Viehland, Magnetoelectric laminate composites: an overview. *J. Am. Ceram. Soc.* **91**(2), 351–358 (2008)
15. S. Picozzi, C. Ederer, First principles studies of multiferroic materials. *J. Phys.: Condens. Matter* **21**(30), 303201–303237 (2009)
16. M. Vopsaroiu, J. Blackburn, M.G. Cain, Emerging technologies and opportunities based on the magneto-electric effect in multiferroic composites. *MRS Proc.* **1161**, 1161-I05-04 (2009)
17. J. Ryu, S. Priya, K. Uchino, H.-E. Kim, Magnetoelectric effect in composites of magnetostrictive and piezoelectric materials. *J. Electroceram.* **8**(2), 107–119 (2002)
18. R.C. Kambale, D.-Y. Jeong, J. Ryu, Current status of magnetoelectric composite thin/thick films. *Adv. Cond. Matter Physics* **2012**, 824643 (2012)
19. G. Lawes, G. Srinivasan, Introduction to magnetoelectric coupling and multiferroic films. *J. Phys. D Appl. Phys.* **44**(24), 243001 (2011)
20. G. Srinivasan, Magnetoelectric composites. *Annu. Rev. Mater. Res.* **40**, 153–178 (2010)
21. L.W. Martin, R. Ramesh, Multiferroic and magnetoelectric heterostructures. *Acta Mater.* **60** (6–7), 2449–2470 (2012)
22. S. Priya, R. Islam, S. Dong, D. Viehland, Recent advancements in magnetoelectric particulate and laminate composites. *J. Electroceram.* **19**(1), 149–166 (2007)
23. J. Ma, J. Hu, Z. Li, C.-W. Nan, Recent progress in multiferroic magnetoelectric composites: from bulk to thin films. *Adv. Mater.* **23**(9), 1062–1087 (2011)
24. M. Bichurin, V. Petrov, A. Zakharov, D. Kovalenko, S.C. Yang, D. Maurya, V. Bedekar, S. Priya, Magnetoelectric interactions in lead-based and lead-free composites. *Materials* **4**(4), 651–702 (2011)
25. R. Grössinger, G.V. Duong, R. Sato-Turtelli, The physics of magnetoelectric composites. *J. Mag. Mag. Mat.* **320**(14), 1972–1977 (2008)
26. Ü. Özgür, Y. Alivov, H. Morkoç, Microwave ferrites, part 2: passive components and electrical tuning. *J. Mater. Sci.: Mater. Electron.* **20**(10), 911–951 (2009)
27. T.H. O'Dell, The field invariants in a magneto-electric medium. *Phil. Mag.* **8**(87), 411–418 (1963)
28. M.I. Bichurin, V.M. Petrov, D.A. Filippov, G. Srinivasan, *Magnetoelectric Effect in Composite Materials (em russo)*. Veliki Noogorod (2005)
29. W.F. Brown, Jr., R.M. Hornreich, S. Shtrikman, Upper bound on the magnetoelectric susceptibility. *Phys. Rev.* **168**(2), 574–577 (1968)
30. N.A. Spaldin, R. Ramesh, Electric-field control of magnetism in complex oxide thin films. *MRS Bull.* **33**, 1047–1050 (2008)
31. G.A. Gehring, On the microscopic theory of the magnetoelectric effect. *Ferroelectrics* **161**(1), 275–285 (1994)
32. N.A. Hill, Why are there so few magnetic ferroelectrics? *J. Phys. Chem. B* **104**(29), 6694–6709 (2000)
33. J.-P. Rivera, A short review of the magnetoelectric effect and related experimental techniques on single phase (multi-) ferroics. *Eur. Phys. J. B* **71**(3), 299–313 (2009)
34. J.P. Rivera, On definitions, units, measurements, tensor forms of the linear magnetoelectric effect and on a new dynamic method applied to Cr-Cl boracite. *Ferroelectrics* **161**(1), 165–180 (1994)
35. H. Grimmer, The forms of tensors describing magnetic, electric and toroidal properties. *Ferroelectrics* **161**(1), 181–189 (1994)
36. R.A. Islam, S. Priya, Progress in dual (Piezoelectric-Magnetostrictive) phase magnetoelectric sintered composites. *Adv. Cond. Matter Phys.* **2012**, 1–29 (2012)

37. J.V. Suchtelen, Product properties: a new application of composite materials. *Philips Res. Rep.* **27**(1), 28–37 (1972)
38. J.V.D. Boomgard, A.M.J.G.V. Run, J.V. Suchtelen, Piezoelectric-piezomagnetic composites with magnetoelectric effect. *Ferroelectrics* **14**(1), 727–728 (1976)
39. C.-W. Nan, Magnetoelectric effect in composites of piezoelectric and piezomagnetic phases. *Phys. Rev. B* **50**(9), 6082–6088 (1994)
40. D.C. Lupascu, H. Wende, M. Etier, A. Nazrabi, I. Anusca, H. Trivedi, V.V. Shvartsman, J. Landers, S. Salamon, C. Schmitz-Antoniak, Measuring the magnetoelectric effect across scales. *GAMM-Mitteilungen* **38**(1), 25–74 (2015)
41. C.-W. Nan, Physics of inhomogeneous inorganic materials. *Prog. Mater. Sci.* **37**(1), 1–116 (1993)
42. M.I. Bichurin, V.M. Petrov, G. Srinivasan, Theory of low-frequency magnetoelectric effects in ferromagnetic-ferroelectric layered composites. *J. Appl. Phys.* **92**(12), 7681–7683 (2002)
43. M.I. Bichurin, V.M. Petrov, G. Srinivasan, Theory of low-frequency magnetoelectric coupling in magnetostrictive-piezoelectric bilayers. *Phys. Rev. B* **68**(5), 054402–054414 (2003)
44. G.V. Duong, R. Groessinger, M. Schoenbart, D. Bueno-Basques, The lock-in technique for studying magnetoelectric effect. *J. Mag. Mag. Mat.* **316**(2), 390–393 (2007)
45. X. Zhuang, M.L.C. Sing, C. Cordier, S. Saez, C. Dolabdjian, J. Das, J. Gao, J. Li, D. Viehland, Analysis of noise in magnetoelectric thin-layer composites used as magnetic sensors. *IEEE Sens. J.* **11**(10), 2183–2188 (2011)
46. Y.J. Wang, J.Q. Gao, M.H. Li, Y. Shen, D. Hasanyan, J.F. Li, D. Viehland, A review on equivalent magnetic noise of magnetoelectric laminate sensors. *Phil. Trans. R. Soc. A* **372**(2009), 20120455 (2014)
47. Z.P. Xing, J.Y. Zhai, S.X. Dong, J.F. Li, D. Viehland, W.G. Odendaal, Modeling and detection of quasi-static nanoscale magnetic field variations using magnetoelectric laminate sensors. *Meas. Sci. Technol.* **19**(1), 015206–015214 (2008)
48. Y. Wang, D. Gray, D. Berry, J. Gao, M. Li, J. Li, D. Viehland, An extremely low equivalent magnetic noise magnetoelectric sensor. *Adv. Mater.* **23**(35), 4111–4114 (2011)
49. R. Jahns, H. Greve, E. Woltermann, E. Quandt, R.H. Knochel, Noise performance of magnetometers with resonant thin-film magnetoelectric sensors. *IEEE T. Instrum. Meas.* **60**(8), 2995–3001 (2011)
50. R.E. Newnham, D.P. Skinner, L.E. Cross, Connectivity and piezoelectric-pyroelectric composites. *Mater. Res. Bull.* **13**(5), 525–536 (1978)
51. S.N. Babu, T. Bhimasankaram, S.V. Suryanarayana, Magnetoelectric effect in metal-PZT laminates. *Bull. Mater. Sci.* **28**(5), 419–422 (2004)
52. C.P. Zhao, F. Fang, W. Yang, A dual-peak phenomenon of magnetoelectric coupling in laminated Terfenol-D/PZT/Terfenol-D composites. *Smart Mater. Struct.* **19**(12), 125004–125010 (2010)
53. J. Ryu, A.V. Carazo, K. Uchino, H.-E. Kim, Magnetoelectric properties in piezoelectric and magnetostrictive laminate composites. *Jpn. J. Appl. Phys.* **40**(8), 4948–4951 (2001)
54. IEEE Standard on Piezoelectricity. *ANSI/IEEE Std 176-1987*, pp. 1–74 (1988)
55. M. Zgonik, P. Bernasconi, M. Duelli, R. Schlessler, P. Günter, M.H. Garrett, D. Rytz, Y. Zhu, X. Wu, Dielectric, elastic, piezoelectric, electro-optic, and elasto-optic tensors of BaTiO₃ crystals. *Phys. Rev. B* **50**(9), 5941–5949 (1994)
56. H. Xiao-Kang, Z. Li-Bo, W. Qiong-Shui, Z. Li-Yan, Z. Ke, L. Yu-Long, Determination of elastic, piezoelectric, and dielectric constants of an R:BaTiO₃ single crystal by Brillouin scattering. *Chin. Phys. B* **21**(6), 067801 (2012)
57. R.S. Weis, T.K. Gaylord, Lithium niobate: summary of physical properties and crystal structure. *Appl. Phys. A Mater. Sci. Process.* **37**(4), 191–203 (1985)
58. P. Davulis, J.A. Kosinski, M.P. da Cunha, GaPO₄ stiffness and piezoelectric constants measurements using the combined thickness excitation and lateral field technique. in *International Frequency Control Symposium and Exposition, 2006 IEEE*, 664–669 (2006)

59. W. Wallnöfer, P.W. Krempf, A. Asenbaum, Determination of the elastic and photoelastic constants of quartz-type GaPO₄ by Brillouin scattering. *Phys. Rev. B* **49**(15), 10075–10080 (1994)
60. M. Šulca, J. Erharta, J. Noseka, Interferometric measurement of the temperature dependence of piezoelectric coefficients for PZN-8 %PT single crystals. *Ferroelectrics* **293**(1), 283–290 (2003)
61. D.-S. Paik, S.-E. Park, T.R. ShROUT, W. Hackenberger, Dielectric and piezoelectric properties of perovskite materials at cryogenic temperatures. *J. Mater. Sci.* **34**(3), 469–473 (1999)
62. M. Shanthi, L.C. Lim, K.K. Rajan, J. Jin, Complete sets of elastic, dielectric, and piezoelectric properties of flux-grown [011]-poled Pb(Mg₁/3Nb₂/3)O₃-(28–32)%PbTiO₃ single crystals. *Appl. Phys. Lett.* **92**(14), 142906 (2008)
63. S.S. Guo, S.G. Lu, Z. Xu, X.Z. Zhao, S.W. Or, Enhanced magnetoelectric effect in Terfenol-D and flextensional cymbal laminates. *Appl. Phys. Lett.* **88**(18), 182906–182908 (2006)
64. J.G. Wan, Z.Y. Li, Y. Wang, M. Zeng, G.H. Wang, J.-M. Liu, Strong flexural resonant magnetoelectric effect in Terfenol-D/epoxy-Pb(Zr, Ti)O₃ bilayer. *Appl. Phys. Lett.* **86**(20), 202504–202506 (2005)
65. S. Dong, J.-F. Li, D. Viehland, Longitudinal and transverse magnetoelectric voltage coefficients of magnetostrictive/piezoelectric laminate composite: theory. *IEEE Trans. Ultrason. Ferroelectr. Freq. Control* **50**(10), 1253–1261 (2003)
66. S. Dong, J.-F. Li, D. Viehland, Ultrahigh magnetic field sensitivity in laminates of TERFENOL-D and Pb(Mg₁/3Nb₂/3)O₃-PbTiO₃ crystals. *Appl. Phys. Lett.* **83**(11), 2265–2267 (2003)
67. S. Dong, J. Cheng, J.F. Li, D. Viehland, Enhanced magnetoelectric effects in laminate composites of Terfenol-D/Pb(Zr, Ti)O₃ under resonant drive. *Appl. Phys. Lett.* **83**(23), 4812–4814 (2003)
68. J. Zhai, S. Dong, Z. Xing, J. Li, D. Viehland, Giant magnetoelectric effect in Metglas/polyvinylidene-fluoride laminates. *Appl. Phys. Lett.* **89**(8), 083507–083509 (2006)
69. Y. Yang, J. Gao, Z. Wang, M. Li, J.-F. Li, J. Das, D. Viehland, Effect of heat treatment on the properties of Metglas foils, and laminated magnetoelectric composites made thereof. *Mater. Res. Bull.* **46**(2), 266–270 (2011)
70. U. Laletsin, N. Padubnaya, G. Srinivasan, C.P. DeVreugd, Frequency dependence of magnetoelectric interactions in layered structures of ferromagnetic alloys and piezoelectric oxides. *Appl. Phys. A* **78**(1), 33–36 (2004)
71. http://www.metglas.com/products/magnetic_materials/
72. S. Dong, J. Zhai, J. Li, D. Viehland, Near-ideal magnetoelectricity in high-permeability magnetostrictive/piezofiber laminates with a (2-1) connectivity. *Appl. Phys. Lett.* **89**(25), 252904–252906 (2006)
73. G. Sreenivasulu, S.K. Mandal, S. Bandekar, V.M. Petrov, G. Srinivasan, Low-frequency and resonance magnetoelectric effects in piezoelectric and functionally stepped ferromagnetic layered composites. *Phys. Rev. B* **84**(14), 144426–144431 (2011)
74. J. Wang, Y. Zhang, J. Ma, Y. Lin, C.W. Nan, Magnetoelectric behavior of BaTiO₃ films directly grown on CoFe₂O₄ ceramics. *J. Appl. Phys.* **104**(1), 014101–014105 (2008)
75. T. Kiyomiya, Y. Yamada, Y. Matsuo, H. Wakiwaka, Y. Torii, M. Makimura, Magnetostrictive properties of Tb-Fe and Tb-Fe-Co films. *Electron. Comm. Jpn.* **91**(5), 49–55 (2008)
76. G. Sreenivasulu, U. Laletin, V.M. Petrov, V.V. Petrov, G. Srinivasan, A permendur-piezoelectric multiferroic composite for low-noise ultrasensitive magnetic field sensors. *Appl. Phys. Lett.* **100**(17), 173506–173510 (2012)
77. M. Matsumoto, T. Kubota, M. Yokoyama, T. Okazaki, Y. Furuya, A. Makino, M. Shimada, Magnetic properties of rapidly solidified ribbon of Fe₄₉Co₄₉V₂ and spark-plasma-sintered pellet of its powder. *Mater. Trans.* **51**(10), 1883–1886 (2010)

78. D.A. Burdin, D.V. Chashin, N.A. Ekonomov, L.Y. Fetisov, Y.K. Fetisov, G. Sreenivasulu, G. Srinivasan, Nonlinear magneto-electric effects in ferromagnetic-piezoelectric composites. *J. Mag. Mag. Mat.* **358–359**, 98–104 (2014)
79. A.E. Clark, M. Wun-Fogle, J.B. Restorff, T.A. Lograsso, J.R. Cullen, Effect of quenching on the magnetostriction on $\text{Fe}_{1-x}\text{Ga}_x$ (0.13x < 0.21). *IEEE Trans. Magn.* **37**(4), 2678–2680 (2001)
80. A.E. Clark, M. Wun-Fogle, J.B. Restorff, T.A. Lograsso, Magnetostrictive properties of galphenol alloys under compressive stress. *Mater. Trans.* **43**(5), 881–886 (2002)
81. S. Dong, J.-F. Li, D. Viehland, Magnetolectric coupling, efficiency, and voltage gain effect in piezoelectric-piezomagnetic laminate composites. *J. Mater. Sci.* **41**(1), 97–106 (2006)
82. G. Srinivasan, I.V. Zavislyak, A.S. Tatarenko, Millimeter-wave magnetoelectric effects in bilayers of barium hexaferrite and lead zirconate titanate. *Appl. Phys. Lett.* **89**(15), 152508–152510 (2006)
83. G. Srinivasan, E.T. Rasmussen, J. Gallegos, R. Srinivasan, Y.I. Bokhan, V.M. Laletin, Magnetoelectric bilayer and multilayer structures of magnetostrictive and piezoelectric oxides. *Phys. Rev. B* **64**(21), 214408–214413 (2001)
84. G. Srinivasan, C.P. DeVreugd, C.S. Flattery, V.M. Laletsin, N. Paddubnaya, Magnetoelectric interactions in hot-pressed nickel zinc ferrite and lead zirconate titanate composites. *Appl. Phys. Lett.* **85**(13), 2550–2552 (2004)
85. G. Liu, C.-W. Nan, N. Cai, Y. Lin, Calculations of giant magnetoelectric effect in multiferroic composites of rare-earth-iron alloys and PZT by finite element method. *Int. J. Solids Struct.* **41**(16–17), 4423–4434 (2004)
86. S. Dong, J. Zhai, F. Bai, J.-F. Li, D. Viehland, Push-pull mode magnetostrictive/piezoelectric laminate composite with an enhanced magnetoelectric voltage coefficient. *Appl. Phys. Lett.* **87**(6), 062502–062504 (2005)
87. D.R. Tilley, J.F. Scott, Frequency dependence of magnetoelectric phenomena in BaMnF_4 . *Phys. Rev. B* **25**(5), 3251–3260 (1982)
88. M.I. Bichurin, V.M. Petrov, O.V. Ryabkov, S.V. Averkin, G. Srinivasan, Theory of magnetoelectric effects at magnetoacoustic resonance in single-crystal ferromagnetic-ferroelectric heterostructures. *Phys. Rev. B* **72**(6), 060408–060411 (2005)
89. M.I. Bichurin, V.M. Petrov, Y.V. Kiliba, G. Srinivasan, Magnetic and magnetoelectric susceptibilities of a ferroelectric/ferromagnetic composite at microwave frequencies. *Phys. Rev. B* **66**(13), 134404–134413 (2002)
90. S. Timoshenko, *Vibration Problems in Engineering* (D. Van Nostrand, New York, 1961)
91. U. Laletsin, N. Padubnaya, G. Srinivasan, C.P. DeVreugd, Frequency dependence of magnetoelectric interactions in layered structures of ferromagnetic alloys and piezoelectric oxides. *Appl. Phys. A* **78**(1), 33–36 (2004)
92. Y.K. Fetisov, K.E. Kamentsev, A.Y. Ostashchenko, G. Srinivasan, Wide-band magnetoelectric characterization of a ferrite-piezoelectric multilayer using a pulsed magnetic field. *Solid State Commun.* **132**(1), 13–17 (2004)
93. N. Cai, C.-W. Nan, J. Zhai, Y. Lin, Large high-frequency magnetoelectric response in laminated composites of piezoelectric ceramics, rare-earth iron alloys and polymer. *Appl. Phys. Lett.* **84**(18), 3516–3518 (2004)
94. H. Greve, E. Woltermann, H.-J. Quenzer, B. Wagner, E. Quandt, Giant magnetoelectric coefficients in $(\text{Fe}_{90}\text{Co}_{10})_{78}\text{Si}_{12}\text{B}_{10}\text{-AlN}$ thin film composites. *Appl. Phys. Lett.* **96**(18), 182501–182503 (2010)
95. G. Liu, X. Li, J. Chen, H. Shi, W. Xiao, S. Dong, Colossal low-frequency resonant magnetomechanical and magnetoelectric effects in a three-phase ferromagnetic/elastic/piezoelectric composite. *Appl. Phys. Lett.* **101**(14), 142904–142907 (2012)
96. H. Greve, E. Woltermann, R. Jahns, S. Marauska, B. Wagner, R. Knöchel, M. Wuttig, E. Quandt, Low damping resonant magnetoelectric sensors. *Appl. Phys. Lett.* **97**(15), 152503–152505 (2010)

97. Y. Zhang, G. Liu, H. Shi, W. Xiao, Y. Zhu, M. Li, M. Li, J. Liu, Enhanced magnetoelectric effect in ferromagnetic–elastic–piezoelectric composites. *J. Alloy. Compd.* **613**, 93–95 (2014)
98. M. Liu, O. Obi, J. Lou, Y. Chen, Z. Cai, S. Stoute, M. Espanol, M. Lew, X. Situ, K.S. Ziemer, V.G. Harris, N.X. Sun, Giant electric field tuning of magnetic properties in multiferroic ferrite/ferroelectric heterostructures. *Adv. Funct. Mater.* **19**(11), 1826–1831 (2009)
99. S. Sherrit, B.K. Mukherjee, *Characterization of Piezoelectric Materials for Transducers*, arXiv (2007)
100. W.P. Mason, *Physical Acoustics and the Properties of Solids (The Bell Telephone Laboratories Series)* (Van Nostrand, 1958)
101. T. Ikeda, *Fundamentals of Piezoelectricity* (Oxford Science Publications, 1990)
102. J.W. Morris, *Notes on the Thermodynamics of Solids (Chapter 15: Tensors and Tensor Properties)* (Department of Materials Science and Engineering, University of California, Berkeley, 2008)
103. D. Damjanovic, Ferroelectric, dielectric and piezoelectric properties of ferroelectric thin films and ceramics. *Rep. Prog. Phys.* **61**(9), 1267 (1998)
104. R.F. Tinder, *Tensor Properties of Solids: Phenomenological Development of the Tensor Properties of Crystals* (Morgan & Claypool Publishers, 2008)
105. J.F. Nye, *Physical Properties of Crystals: Their Representation by Tensors and Matrices* (Oxford University Press, 1985)
106. IRE Standards on Piezoelectric Crystals: Determination of the Elastic, Piezoelectric, and Dielectric Constants-The Electromechanical Coupling Factor, 1958. *Proc. IRE* **46**(4), 764–778 (1958)
107. H.-Y. Kuo, A. Slinger, K. Bhattacharya, Optimization of magnetoelectricity in piezoelectric–magnetostrictive bilayers. *Smart Mater. Struct.* **19**(12), 125010–125022 (2010)
108. D.A. Burdin, D.V. Chashin, N.A. Ekonomov, L.Y. Fetisov, Y.K. Fetisov, G. Sreenivasulu, G. Srinivasan, Nonlinear magneto-electric effects in ferromagnetic-piezoelectric composites. *J. Mag. Mag. Mat.* **358–359**, 98–104 (2014)
109. Y. Benveniste, Magnetolectric effect in fibrous composites with piezoelectric and piezomagnetic phases. *Phys. Rev. B* **51**(22), 16424–16427 (1995)
110. C.W. Nan, M. Li, J.H. Huang, Calculations of giant magnetoelectric effects in ferroic composites of rare-earth–iron alloys and ferroelectric polymers. *Phys. Rev. B* **63**(14), 144415 (2001)
111. R. Tinder, *Tensor Properties of Solids* (Morgan & Claypool, 2007)
112. J.A. Osborn, Demagnetizing factors of the general ellipsoid. *Phys. Rev.* **67**(11–12), 351–357 (1945)
113. A.A. Timopheev, J.V. Vidal, A.L. Kholkin, N.A. Sobolev, Direct and converse magnetoelectric effects in Metglas/LiNbO₃/Metglas trilayers. *J. Appl. Phys.* **114**(4), 044102–044108 (2013)
114. Y. Wang, S.W. Or, H.L.W. Chan, X. Zhao, H. Luo, Enhanced magnetoelectric effect in longitudinal-transverse mode Terfenol-D/Pb(Mg_{1/3}Nb_{2/3})O₃–PbTiO₃ laminate composites with optimal crystal cut. *J. Appl. Phys.* **103**(12), 124511 (2008)
115. C.-S. Park, K.-H. Cho, M.A. Arat, J. Evey, S. Priya, High magnetic field sensitivity in Pb(Zr, Ti)O₃–Pb(Mg_{1/3}Nb_{2/3})O₃ single crystal/Terfenol-D/Metglas magnetoelectric laminate composites. *J. Appl. Phys.* **107**(9), 094109 (2010)
116. J. Lou, M. Liu, D. Reed, Y. Ren, N.X. Sun, Giant Electric Field Tuning of Magnetism in Novel Multiferroic FeGaB/Lead Zinc Niobate-Lead Titanate (PZN-PT) Heterostructures. *Adv. Mater.* **21**(46), 4711–4715 (2009)
117. H.F. Tian, T.L. Qu, L.B. Luo, J.J. Yang, S.M. Guo, H.Y. Zhang, Y.G. Zhao, J.Q. Li, Strain induced magnetoelectric coupling between magnetite and BaTiO₃. *Appl. Phys. Lett.* **92**(6), 063507–063509 (2008)

118. P. Yang, K. Zhao, Y. Yin, J.G. Wan, J.S. Zhu, Magnetoelectric effect in magnetostrictive/piezoelectric laminate composite Terfenol-D/LiNbO₃ [(zxtw) – 129°/30°]. *Appl. Phys. Lett.* **88**(17), 172903–172905 (2006)
119. J.V. Vidal, A.A. Timopheev, A.L. Kholkin, N.A. Sobolev, Anisotropy of the magnetoelectric effect in tri-layered composites based on single-crystalline piezoelectrics. *Vacuum*, 1–7
120. G. Sreenivasulu, V.M. Petrov, L.Y. Fetisov, Y.K. Fetisov, G. Srinivasan, Magnetoelectric interactions in layered composites of piezoelectric quartz and magnetostrictive alloys. *Phys. Rev. B* **86**(21), 214405–214411 (2012)
121. R. Viswan, D. Gray, Y. Wang, Y. Li, D. Berry, J. Li, D. Viehland, Strong magnetoelectric coupling in highly oriented ZnO films deposited on Metglas substrates. *Phys. Status Solidi-R* **5**(10–11), 391–393 (2011)
122. G. Sreenivasulu, L.Y. Fetisov, Y.K. Fetisov, G. Srinivasan, Piezoelectric single crystal langatate and ferromagnetic composites: Studies on low-frequency and resonance magnetoelectric effects. *Appl. Phys. Lett.* **100**(5), 052901–052904 (2012)
123. G. Sreenivasulu, P. Qu, E. Piskulich, V.M. Petrov, Y.K. Fetisov, A.P. Nosov, H. Qu, G. Srinivasan, Shear strain mediated magneto-electric effects in composites of piezoelectric lanthanum gallium silicate or tantalate and ferromagnetic alloys. *App. Phys. Lett.* **105**(3), 032409–032412 (2014)
124. F. Fang, C. Zhao, W. Yang, Thickness effects on magnetoelectric coupling for Metglas/PZT/Metglas laminates. *Sci. China Phys. Mech. Astron.* **54**(4), 581–585 (2011)
125. D. Hasanyan, J. Gao, Y. Wang, R. Viswan, Y.S.M. Li, J. Li, D. Viehland, Theoretical and experimental investigation of magnetoelectric effect for bending-tension coupled modes in magnetostrictive-piezoelectric layered composites. *J. Appl. Phys.* **112**(1), 013908–013918 (2012)
126. Y. Wang, D. Hasanyan, M. Li, J. Gao, J. Li, D. Viehland, H. Luo, Theoretical model for geometry-dependent magnetoelectric effect in magnetostrictive/piezoelectric composites. *J. Appl. Phys.* **111**(12), 124513–124518 (2012)
127. <http://bostonpiezooptics.com/crystal-quartz>
128. R.T. Smith, F.S. Welsh, Temperature dependence of the elastic, piezoelectric, and dielectric constants of lithium tantalate and lithium niobate. *J. Appl. Phys.* **42**(6), 2219–2230 (1971)
129. A. Balatto, Basic Material Quartz and Related Innovations. *Springer Series in Materials Science*, **114**, 9–35 (2008)
130. J. Kushibiki, I. Takanaga, S. Nishiyama, Accurate measurements of the acoustical physical constants of synthetic/spl alpha/-quartz for SAW devices. *IEEE Trans. Ultrason. Ferroelectr. Freq. Control* **49**(1), 125–135 (2002)
131. P.M. Davulis, M.P.D. Cunha, A full set of langatate high-temperature acoustic wave constants: elastic, piezoelectric, dielectric constants up to 900 °C. *IEEE Trans. Ultrason., Ferroelectr., Freq. Control.* **60**(4), 824–33 (2013)
132. Y.K. Fetisov, D.A. Burdin, D.V. Chashin, N.A. Ekonomov, High-Sensitivity Wideband Magnetic Field Sensor Using Nonlinear Resonance Magnetoelectric Effect. *Sens. J., IEEE* **14**(7), 2252–2256 (2014)
133. M. Adachi, T. Kimura, W. Miyamoto, Z. Chen, A. Kawabata, Dielectric, elastic and piezoelectric properties of La₃Ga₅SiO₁₄ (LANGASITE) single crystals. *J. Korean Phys. Soc.* **32**, S1274–S1277 (1998)
134. R. Tarumi, H. Nitta, H. Ogi, M. Hirao, Low-temperature elastic constants and piezoelectric coefficients of langasite (La₃Ga₅SiO₁₄). *Philos. Mag.* **91**(16), 2140–2153 (2011)
135. A. Sotnikov, H. Schmidt, M. Weihnacht, E. Smirnova, T. Chemekova, Y. Makarov, Elastic and piezoelectric properties of AlN and LiAlO₂ single crystals. *IEEE Trans. Ultrason. Ferroelectr. Freq. Control* **57**(4), 808–811 (2010)
136. G. Bu, D. Ciplys, M. Shur, L.J. Schowalter, S. Schujman, R. Gaska, Electromechanical coupling coefficient for surface acoustic waves in single-crystal bulk aluminum nitride. *Appl. Phys. Lett.* **84**(23), 4611–4613 (2004)
137. <http://www.roditi.com/SingleCrystal/Lithium-Tantalate/LiTaO3-Properties.html>

138. R.T. Smith, F.S. Welsh, Temperature dependence of the elastic, piezoelectric, and dielectric constants of lithium tantalate and lithium niobate. *J. Appl. Phys.* **42**(6), 2219–2230 (1971)
139. A.W. Warner, M. Onoe, G.A. Coquin, Determination of elastic and piezoelectric constants for crystals in class (3 m). *J. Acoust. Soc. America* **42**(6), 1223–1231 (1967)
140. Technical Publication TP-226 - Properties of Piezoelectricity Ceramics, Morgan Electro Ceramics
141. R. Zhang, B. Jiang, W. Cao, Single-domain properties of $0.67\text{Pb}(\text{Mg}_{1/3}\text{Nb}_{2/3})\text{O}_3$ – 0.33PbTiO_3 single crystals under electric field bias. *Appl. Phys. Lett.* **82**(5), 787–789 (2003)
142. R. Zhang, B. Jiang, W. Cao, Elastic, piezoelectric, and dielectric properties of multidomain $0.67\text{Pb}(\text{Mg}_{1/3}\text{Nb}_{2/3})\text{O}_3$ – 0.33PbTiO_3 single crystals. *J. Appl. Phys.* **90**(7), 3471–3475 (2001)
143. C. He, J. Weiping, W. Feifei, K. Zhu, Q. Jinhao, Full tensorial elastic, piezoelectric, and dielectric properties characterization of [011]-poled PZN-9 %PT single crystal. *IEEE Trans. Ultrason. Ferroelectr. Freq. Control* **58**(6), 1127–1130 (2011)
144. R. Zhang, B. Jiang, W. Cao, Complete set of properties of $0.92\text{Pb}(\text{Zn}_{1/3}\text{Nb}_{2/3})\text{O}_3$ – 0.08PbTiO_3 single crystal with engineered domains. *Mater. Lett.* **57**(7), 1305–1308 (2003)
145. H.-M. Zhou, Y.-H. Zhou, X.-J. Zheng, Q. Ye, J. Wei, A general 3-D nonlinear magnetostrictive constitutive model for soft ferromagnetic materials. *J. Mag. Mag. Mat.* **321**(4), 281–290 (2009)